2015

Wireless Localization in the Absence of GPS

Hyundeok Kang
Louisiana State University and Agricultural and Mechanical College, hkang8@lsu.edu

WIRELESS LOCALIZATION IN THE ABSENCE OF GPS

A Thesis

Submitted to the Graduate Faculty of the
Louisiana State University and
Agricultural and Mechanical College
in partial fulfillment of the
requirements for the degree of
Master of Science in Electrical Engineering

in

The Department of Electrical and Computer Engineering

by
Hyundeok Kang
B.S., Inha University, 2007
M.S., Inha University, 2010
August 2016

ACKNOWLEDGEMENTS

First of all, this work was supported by the AFRL Minority Leaders-Research Collaboration Program, contract FA8650-13-5800. I greatly acknowledge the following individuals for their assistance in this work: Dr. Robert Ewing, AFRL/RY and Dr. Alan Karrick, AFRL/RY.

I would like to express my sincere thanks to Dr. Guoxiang Gu for giving me the opportunity to do my Master thesis. Because of his continuous support, his kind, helpful advice and to the interesting discussions, I was able to stay focused and not stray away from the essence of my work.

I would like to thank my committee members, Dr. Martin Feldman and Dr. Morteza Naraghi-Pour, for taking time out of their busy schedules and consenting to be a part of my committee, and for their valuable feedback.

In addition, I would like to thank the faculty, staff, and students in the Department of Electrical and Computer Engineering for all the help and support I have received.

I would also like to thank my family and friends who put their faith in me and urged me to do better.

TABLE OF CONTENTS

ABSTRACT

In this thesis, wireless localization is investigated based on multiple noisy estimates of the time-difference of arrival (TDOA) at each pair of the $n \geq 4$ sensors with different but known locations using WiFi opportunistic signals.

Our work is comprehensive and includes channel estimation, symbol detection, TDOA estimation, and location estimation. To mitigate the multipath issue induced by wideband signals, such as WiFi, frequency-division is employed to decompose the wideband RF signal into multiple non-overlapping narrowband signals. To minimize the adverse effects of the clock drift, time-division is proposed to divide the signal into multiple non-overlapping signals in the time domain. In addition, Kalman filtering is proposed, assuming the wide-sense stationary and uncorrelated scattering (WSSUS) channel and the first order auto-regressive (AR) model are used. Because of the multiple TDOA estimates at each pair of the WiFi receiver sensors, an efficient algorithm is developed to estimate the target location. The localization technique developed in this thesis can also be extended to other radio frequency (RF) signals, as shown in our simulation study for out-door localization.

The simulation results in our thesis show the effectiveness of the wireless localization, although further work is needed to resolve the nonlinear estimation problem involved in localization based on TDOA estimates.

CHAPTER 1
INTRODUCTION

This chapter introduces the wireless localization problem and the related works in this problem area. Our thesis work will be briefly discussed and followed by a summary of each chapter.

1.1 Overview and Related Work

Passive source localization has been an important research topic in the signal processing society and received the renewed interest due to the attention to localization based on wireless networks. See for instance [15] and the references therein. Even though the success of the global positioning system (GPS) diminished the importance of wireless localization, there are needs for developing indoor and urban area location systems, because the weak GPS signal cannot penetrate big buildings. Several papers [1], [7], [9], [16], [19] consider source localization based on time-difference of arrival (TDOA) estimates obtained from the radio frequency (RF) signals.

We are motivated to consider wideband RF signals for localization. The study in this thesis can be easily adapted to the case of the WiFi signals [2], [5] that are indeed wideband. However, our localization algorithm is based on the TDOA estimates obtained at the n sensors with different but known locations. Due to the wideband of the RF signals, the multipath phenomena are inevitable. Furthermore, the sensor clocks are mostly based on quartz oscillators, and thus the clock drifting can also be a serious issue for accurate TDOA estimation, which requires a long duration for the observation time of the wideband RF signals. A divide and conquer approach is adopted leading to decomposition of the wideband RF signal into a sum of multiple narrowband signals that are resilient to multipath, and to time division of the received signal over multiple non-overlapping time subintervals in each of which the clock drifting is negligible. Hence we may have $L >> 1$ crude TDOA estimates at each of the n wireless sensors. An assumption for the TDOA estimation errors at the kth

node is the i.i.d. Gauss distribution with mean zero and variance σ_k^2 determined mainly by its signal-to-noise ratio (SNR).

Despite the i.i.d. Gaussian assumption, such a source localization problem is nonlinear in nature and the exact MLE solution is difficult to compute. For this reason, the problem was initially investigated for the case when the sensors are arranged in a linear fashion [1], [3], [9], where different optimum processing techniques are proposed under various assumptions. When the sensors are distributed irregularly, the optimum solutions are much harder to obtain. A linearization approach based on the Taylor series is proposed in [6], [19] to compute the optimum solution iteratively. Because of the existence of local minima, the Taylor series method requires an initial solution close to the global minimum. A more appealing approach is the quasi-linear method employed in [7], [16], [18] that converts the nonlinear measurement equations into quasi-linear measurement equations by treating the nonlinear term as a parameter. Two different procedures are developed independently in [7], [17], which turn out to be mathematically equivalent. Our research results presented in this thesis can also be found in [8], [12], [13] as quarterly reports.

1.2 Thesis Contribution

In this thesis, we take into account the same localization problem using the same quasi-linear measurement equations. Different from the existing solution methods, the nonlinear term in the quasi-linear measurement equations is treated as a constraint that is in fact a quadratic constraint. A numerical procedure based on simultaneous diagonalization [10] is developed to compute the WLS solution under the quadratic constraint. This new procedure is shown to be an approximate MLE solution under a mild assumption that is satisfied so long as the distances from the sensors to the target are not all too small compared to the TDOA estimation errors measured in distance. This thesis also proposes an efficient TDOA estimate method, which uses subband division. The efficient computation to reduce complexity and storage is proposed as well.

1.3 Thesis Organization

This thesis consists of 6 chapters. Chapter 1 is the introduction of our study. Chapter 2 describes OFDM and WiFi, which will be used as a signal for localization purposes. In Chapter 3, the channel estimate and symbol detection procedures using OFDM data transmission are presented. Chapter 4 summarizes the TDOA estimation procedure that will be applied for localization. In Chapter 5, localization based on TDOA is illustrated. Each chapter from Chapters 3 to 5 include the simulation results with specific examples. Lastly, the conclusion is in Chapter 6.

CHAPTER 2
OFDM AND WIFI

In this chapter, we provide an overview and study of orthogonal frequency-division multiplexing (OFDM), adopted in WiFi, which is the local area wireless computer networking technology. Our wireless localization method will be based on WiFi signals.

2.1 OFDM

OFDM has been widely used in wireless communications due to its many advantages. A major advantage is that it can transmit digital messages without intercarrier interference (ICI) and intersymbol interference (ISI) in the multipath environment. Because of multipath propagation, transmitted signals are often distorted at the receiver site. Adding the corrupting noises makes it very difficult to recover the original transmitted symbols. The OFDM is a clever scheme by introducing the cyclic-prefix in the time domain and by taking digital data in the frequency domain. It works very effectively and can efficiently deal with both ISI and ICI, commonly seen in multi-path propagation situations and in broadband radio channels. At the same time, the OFDM transmission technique needs much less computational complexity in the equalization process in each receiver [14]. For these reasons, OFDM is adopted widely as the standard, for instance, in the local area network (LAN) and personal area network (PAN).

2.1.1 Discrete Fourier Transform and Circular Convolution

A major contribution of the OFDM is the introduction of discrete Fourier transform (DFT) for baseband modulation and demodulation. If the discrete-time signal $\{s_i\}_{i=0}^{N-1}$ is periodic, then DFT can be used to analyze its frequency content:

$$S_k = \frac{1}{\sqrt{N}} \sum_{i=0}^{N-1} s_i W_N^{ik}, \quad W_N = e^{-j2\pi/N},$$

where $0 \leq k \leq N-1$. There exists a fast algorithm for computing DFT called FFT with complexity $\mathcal{O}(N \log_2(N))$. For the two discrete-time periodic signals $\{f_i\}_{i=0}^{N-1}$ and $\{g_i\}_{i=0}^{N-1}$, we can define circular convolution as

$$s_i = f_i \circledast g_i = \sum_{k=0}^{N-1} f_k g_{i-k}, \quad i = 0, 1, \cdots, N-1.$$

Let $\{F_k\}_{k=0}^{N-1}$ and $\{G_k\}_{k=0}^{N-1}$ be the DFT of $\{f_i\}_{i=0}^{N-1}$ and $\{g_i\}_{i=0}^{N-1}$, respectively. It follows from the properties of the DFT that is

$$S_k = F_k G_k, \quad k = 0, 1, \cdots, N-1. \tag{2.1}$$

We cannot compute circular convolutions that requires N^2 multiplications. However, it can be implemented by FFTs for $\{f_i\}_{i=0}^{N-1}$ and $\{g_i\}_{i=0}^{N-1}$, then (2.1) plus inverse FFT. So, we need only $N + \frac{3}{2}N \log_2(N)$ multiplications. The use of FFT greatly reduces the computational complexity in the case of large N. Moreover FFT is numerically reliable and efficient.

2.1.2 Use of FFT for Linear Convolution

If we have two non-periodic sequences $\{f_i\}_{i=0}^{n-1}$ and $\{g_i\}_{i=0}^{m-1}$, its linear convolution is (assuming that $n \leq m$):

$$s_i = f_i * \ g_i = \sum_{k=0}^{n-1} f_k g_{i-k}, \quad i = 0, 1, \cdots, n+m-2. \tag{2.2}$$

Direct computation requires Nn multiplications with $N = n+m-1$. But the FFT approach needs only $N + \frac{3}{2}N \log_2(N)$ multiplications. We can use zero-padding to form $\{f_i\}_{i=0}^{N-1}$ and $\{g_i\}_{i=0}^{N-1}$ and extend the sequences into the periodic ones. Then in the fundamental period, the results coincide with those in (2.2). For $n = m = 128$, the direct method requires $2 \times 128^2 = 32,768$, while the FFT method requires $3,328$. So, the reduction is roughly a factor of 10 (no reduction if $n = N/10 = 12.8$). The DFT matrix is unitary, which is

numerically stable for its multiplication with vectors:

$$\begin{bmatrix} S_0 \\ S_1 \\ \vdots \\ S_{N-1} \end{bmatrix} = T_{\text{DFT}} \begin{bmatrix} s_0 \\ s_1 \\ \vdots \\ s_{N-1} \end{bmatrix}, \quad T_{\text{DFT}} := \frac{1}{\sqrt{N}} \begin{bmatrix} 1 & 1 & 1 & \cdots & 1 \\ 1 & W_N^1 & W_N^2 & \cdots & W_N^{N-1} \\ \vdots & \vdots & \vdots & \cdots & \vdots \\ 1 & W_N^{N-1} & W_N^{2(N-1)} & \cdots & W_N^{(N-1)^2} \end{bmatrix}.$$

2.1.3 From Multipath to AWGN Channels

For a wireless multipath channel, its output is given by

$$\begin{aligned} y(n) &= h(n) * s(n) = \sum_{i=0}^{\ell} h(i)s(n-i) \\ &= h(0)s(n) + h(1)s(n-1) + \cdots + h(\ell)s(n-\ell) \end{aligned}$$

which is a linear convolution. The detection of $s(n)$ needs to overcome the ISI. The idea is to replace the linear convolution by circular convolution using zero-padding (which will be replaced by the cyclic prefix). We transmit the data in the block of the fixed size $L >> \ell$, and insert at least ℓ zeros at the beginning of the block, which is now $\{s(n)\}_{n=0}^{N-1}$, and has size $N \geq L + \ell$. Suppose that $\{S_k\}_{k=0}^{N-1}$ is the N-point DFT of $\{s(n)\}_{n=0}^{N-1}$, and $\{H_k\}_{k=0}^{N-1}$ is the N-point DFT of $\{s(n)\}_{n=0}^{N-1}$. Then FFT of the output $\{y(n)\}_{n=0}^{N-1}$ gives

$$Y_k = H_k S_k + N_k, \quad k = 0, 1, \cdots, N-1.$$

So we have the so called AWGN channel for each k, in which the ISI is completely eliminated. The data rate suffers by a factor of ℓ/N, which is insignificant, if $N >> \ell$.

2.1.4 Cyclic Prefix

The introduction of the cyclic prefix (CP) solves the orthogonality problem. Our data are $\{x_k\}_{k=0}^{N-1} = \{S_k\}_{k=0}^{N-1}$, which are actually in the frequency domain. So, we first apply inverse DFT to obtain $\{s(i)\}_{i=0}^{N-1}$ in the time domain. This is also called an IDFT modulation.

Then we augment the sequence into $\{s(i)\}_{i=0}^{N+\ell}$ by adding the last ℓ data to the beginning, as illustrated here:

$$s(N-\ell), \cdots, s(N-1), s(0), s(1), \cdots, s(N-\ell), \cdots, s(N-1).$$

The received signal is (we have removed the CP):

$$\begin{aligned} y(\ell+n) &= \sum_{k=0}^{\ell-1} h(k)s(n+\ell-k), \quad n=0,1,\cdots,N-1, \\ \Longrightarrow \quad & \begin{bmatrix} y(\ell) \\ \vdots \\ y(N+\ell-1) \end{bmatrix} = T_C \begin{bmatrix} s(0) \\ \vdots \\ s(N-1) \end{bmatrix} \end{aligned} \tag{2.3}$$

where T_C is a Toeplitz matrix, given by

$$T_C = \begin{bmatrix} h(0) & 0 & \cdots & 0 & h(\ell) & \cdots & h(1) \\ h(1) & \ddots & \ddots & \ddots & \ddots & \ddots & \vdots \\ \vdots & \ddots & \ddots & \ddots & \ddots & \ddots & h(\ell) \\ h(\ell) & \ddots & \ddots & \ddots & \ddots & \ddots & 0 \\ 0 & \ddots & \ddots & \ddots & \ddots & \ddots & \vdots \\ \vdots & \ddots & \ddots & \ddots & \ddots & \ddots & 0 \\ 0 & \ddots & 0 & h(\ell) & \cdots & h(1) & h(0) \end{bmatrix} \tag{2.4}$$

2.1.5 Circulant Matrix

The Toeplitz matrix T_C is the size $N \times N$ and is called circulant because each row is a circular rotation (to the right) of the previous row. Such a matrix can be diagonalized by the DFT matrix:

$$\text{diag}(H_0, H_1, \cdots, H_{N-1}) = \mathbf{W}_F T_C \mathbf{W}_F^{-1} = \mathbf{W}_F T_C \mathbf{W}_F^*,$$

where $\mathbf{W}_F$ is the DFT matrix on page 3. Hence multiplying (2.3) from the left by $\mathbf{W}_F$ on both sides, yields

$$\mathbf{W}_F \begin{bmatrix} y(\ell) \\ \vdots \\ y(N+\ell-1) \end{bmatrix} = (\mathbf{W}_F T_C \mathbf{W}_F^*)\mathbf{W}_F \begin{bmatrix} s(0) \\ \vdots \\ s(N-1) \end{bmatrix}.$$

So, we obtain (after taking the noise into account):

$$\begin{bmatrix} Y_0 \\ \vdots \\ Y_{N-1} \end{bmatrix} = \begin{bmatrix} H_0 & & \\ & \ddots & \\ & & H_{N-1} \end{bmatrix} \begin{bmatrix} S_0 \\ \vdots \\ S_{N-1} \end{bmatrix} + \begin{bmatrix} V_0 \\ \vdots \\ V_{N-1} \end{bmatrix}.$$

We again have the AWGN channel: $Y_k = H_k S_k + V_k$ for $0 \leq k < N$.

2.1.6 Discrete-Time Model

Figure 2.1 shows a block diagram of a discrete-time model.

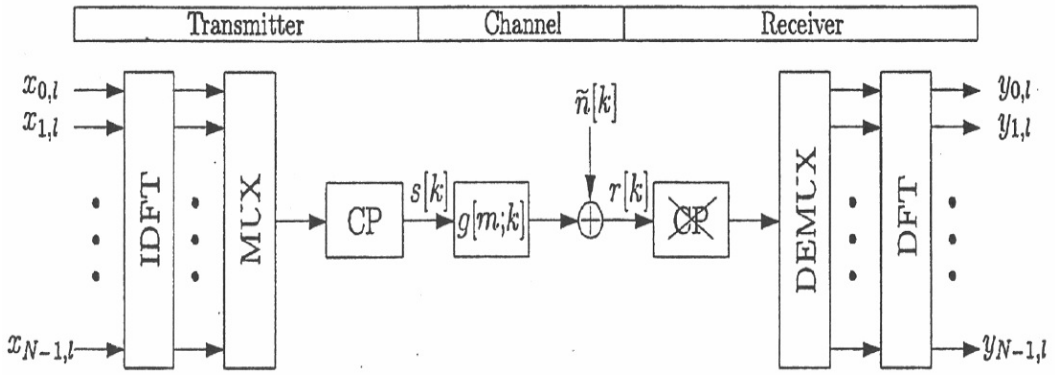

Figure 2.1 Discrete-time model

For the above discrete-time model, we have

$$\begin{aligned} \vec{Y} &= \mathbf{W}_F \left(\vec{\mathbf{h}} \circledast \mathbf{W}_F^*(\vec{S}) + \vec{\mathbf{v}} \right) \\ &= \mathbf{W}_F \left(\vec{\mathbf{h}} \circledast \vec{\mathbf{s}} \right) + \vec{V} = \vec{H} \odot \vec{S} + \vec{V}, \end{aligned}$$

where $\odot$ is the element-wise multiplication of two vectors. The noise vector is Gaussian, white, and uncorrelated.

2.2 WiFi

WiFi is a wireless computer network communication that was invented in order to remedy the disadvantage of a wired LAN. It is widely used for many reasons, such as reducing the work for wired network installation, saving maintenance costs and solving the range limitation of the network.

2.2.1 IEEE 802.11

IEEE 802.11 is a standard for wireless local area network (WLAN) by the LAN/MAN Standards Committee in IEEE. The first version, 802.11-1997, was released in 1997. It provides a maximum data transmission speed of 2 Mbps at the 2.4 GHz band. It was not widely used due to its low speed and there were no strict standards for producing WLAN devices, making them incompatible. In 1999, 802.11a and 802.11b were released. 802.11a uses OFDM for data transmission with a maximum of 54 Mbps at the 5 Ghz band. The advantages are that there is less interference with other devices, such as wireless phones and Bluetooth devices, and has a higher data transmission rate than that of the 2.4 Ghz band. However, its signal strength is reduced easily by its surrounding, such as a wall or other solid objects. On the other hand, 802.11b uses the 2.4 Ghz band and has a maximum data transmission speed of 11 Mbps. It is more practical compared to the previous standards, leading to its wide spread use as a substitute for wired networks at home and companies. In June 2003, 802.11g was released. It uses OFDM and has the same data transmission rate as 802.11a, but it operates at the 2.4 Ghz band. Also, it is compatible with 802.11b. Thus it is very widely used today. For this reason, we focused on the 802.11g standard that uses the 2.4 GHz band and OFDM.

2.2.2 TDOA Estimation Based on WiFi Signals

The 2.4 GHz band is divided into 14 channels spaced 5 MHz apart, beginning with channel 1, which is centered on 2.412 GHz. Figure 2.2 shows WiFi channels in the 2.4 GHz band graphically [20].

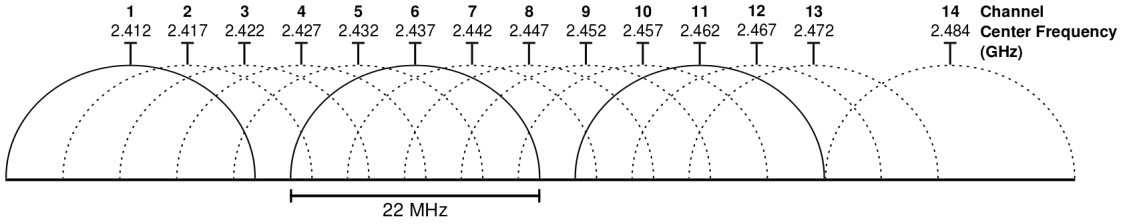

Figure 2.2 WiFi channels in the 2.4 GHz band

The WiFi signals are wideband, and have a bandwidth of 20 MHz. Hence the sampling period is 0.05 microseconds. We use the 64 QAM modulation scheme in this study. So, each OFDM symbol consists of 64 QAM subcarriers in the frequency domain and 3.2 microseconds in the time domain. We divide these 64 QAM subcarriers into 8 subband signals with each occupying 2.5 MHz that make the bandwidth narrower to minimize the adverse effect of multipath. To cope with the clock drift issue, we will divide all the WiFi symbols into different sections with each section consisting of 256 subcarriers corresponding to 4 OFDM symbols. Assume that the neighboring OFDM symbols are separated by 0.5 microseconds. Then the 4 OFDM symbols occupy a total of time interval no more than 15 microseconds, where we assume that the clock drift is negligible. We will assume that TDOA is estimated every 17.5 microseconds. The extra 2.5 microseconds over which no TDOA estimation is made will be used to synchronize the clock in order to initiate a new TDOA estimation.

CHAPTER 3
CHANNEL ESTIMATE AND SYMBOL DETECTION

This chapter summarizes our simulation study for channel estimation and symbol detection using OFDM. The simulation work is one of the components in the simulation studies for localization based on WiFi signals, consisting of not only OFDM, but also estimation of the TDOA and localization based on TDOA estimates. Our simulation is focused on channel estimation and symbol detection in order to recover the transmitted input data in the receiver site with an acceptable error rate.

3.1 Signal and Channel Models

Let $\{S_k\}_{k=0}^{N-1}$ be the subcarriers in the frequency domain to be transmitted. They can be regarded as discrete Fourier transform (DFT) of a sequence $\{s_i\}_{i=0}^{N-1}$ in the time domain. There holds the DFT relation:

$$S_k = \frac{1}{\sqrt{N}} \sum_{i=0}^{N-1} s_i W_N^{ik}, \quad W_N = e^{-j2\pi/N}, \tag{3.1}$$

for $0 \leq k \leq N-1$. Both $\{s_i\}_{i=0}^{N-1}$ and $\{S_k\}_{k=0}^{N-1}$ can be extended to periodic sequences with period N. Given $\{S_k\}_{k=0}^{N-1}$, its inverse DFT (IDFT) is defined by

$$s_i = \frac{1}{\sqrt{N}} \sum_{k=0}^{N-1} S_k W_N^{-ik}, \quad 0 \leq i \leq N-1. \tag{3.2}$$

If $\{s_i\}_{i=0}^{N-1}$ are transmitted over a specified channel, then the received signal is given by

$$y(n) = \sum_{i=0}^{l-1} h_i s(n-i) + v(n) \tag{3.3}$$

where $\{h_i\}_{i=0}^{l-1}$ is the channel impulse response (CIR) for the discretized channel of length l, and $v(t)$ is the corruption noise, resulting in ISI. In order to remove the ISI, the cyclic-prefix is employed by adding the last l subcarriers to the beginning of the sequence. Hence, the

sequence of $\{s_i\}_{i=0}^{N-1}$ are replaced by

$$s(N-l), \cdots, s(N-1), s(0), s(1), \cdots, s(N-l), \cdots, s(N-1).$$

The above leads to a signal and channel model, described by the matrix-vector form:

$$\begin{bmatrix} y(0) \\ \vdots \\ y(N-1) \end{bmatrix} = T_C \begin{bmatrix} s(0) \\ \vdots \\ s(N-1) \end{bmatrix} + \begin{bmatrix} v(0) \\ \vdots \\ v(N-1) \end{bmatrix} \tag{3.4}$$

where T_C is both a circulant and Toeplitz matrix, shown in (2.4). Recall that a circulant matrix is determined by its first row, with every other row obtained by a circular right rotation of the previous row. Let $\{H_k\}_{k=0}^{N-1}$ be the N-point channel frequency response obtained by N-point DFT of the CIR $\{h_i\}_{i=0}^{N-1}$, padded with $h_i = 0$ for $i \geq l$. Then $H_k = H(W_N^{-k})$ where

$$H(z) = \sum_{i=0}^{l-1} h_i z^{-i} = h_0 + h_1 z^{-1} + \cdots + h_{l-1} z^{-(l-1)}$$

is the channel transfer function. It is a fact that the eigenvalue decomposition (EVD) of T_C is given by

$$T_C = T_{\text{DFT}}^* \text{diag}(H_0, H_1, \cdots, H_{N-1}) T_{\text{DFT}}. \tag{3.5}$$

The DFT matrix is an unitary matrix satisfying $T_{\text{DFT}} {T_{\text{DFT}}}^* = I$. Hence, multiplying (3.4) from the left by T_{DFT} on both sides yields

$$\begin{bmatrix} Y(0) \\ \vdots \\ Y(N-1) \end{bmatrix} = T_{\text{DFT}} \begin{bmatrix} y(0) \\ \vdots \\ y(N-1) \end{bmatrix} = T_{\text{DFT}} T_C \begin{bmatrix} s(0) \\ \vdots \\ s(N-1) \end{bmatrix} + T_{\text{DFT}} \begin{bmatrix} v(0) \\ \vdots \\ v(N-1) \end{bmatrix}$$

$$= \begin{bmatrix} H_0 & & \\ & \ddots & \\ & & H_{N-1} \end{bmatrix} \begin{bmatrix} S_0 \\ \vdots \\ S_{N-1} \end{bmatrix} + \begin{bmatrix} V_0 \\ \vdots \\ V_{N-1} \end{bmatrix} \quad \Longrightarrow \quad Y_k = H_s S_k + V_k$$

for $0 \leq k \leq N-1$. The noise $\{V_k\}_{k=0}^{N-1}$ is the N-point DFT of $\{v(i)\}_{i=0}^{N-1}$. Additive white Gaussian noise (AWGN) is a basic channel model widely used in wireless communications to model the random nature of the receiving signal. Under the AWGN assumption, $v(i)$ has a mean of zero and variance of $\sigma_v^2/2$ for both of its real and imaginary parts. In this case we have the so-called Rayleigh fading channel.

Suppose that there are l pilot tones, denoted by $\{S_{km}\}_{k=0}^{l-1}$, that are designed and known to us, where $m = N/l$ is an integer. We can obtain the following relation:

$$\begin{bmatrix} Y_0 \\ Y_m \\ \vdots \\ Y_{(l-1)m} \end{bmatrix} = \begin{bmatrix} H(W_N^{-0})S_0 \\ H(W_N^{-m})S_m \\ \vdots \\ H(W_N^{-(l-1)m})S_{(l-1)m} \end{bmatrix} + \begin{bmatrix} V_0 \\ V_m \\ \vdots \\ V_{(l-1)m} \end{bmatrix}.$$

As a result the maximum likelihood estimate (MLE) for $H_{mm} = H(W_N^{-mm})$ is given by

$$\hat{H}_{km} = \frac{Y_{km}}{S_{km}}, \qquad k = 0, 1, \cdots, l-1. \tag{3.6}$$

The CIR estimates $\{\hat{h}_i\}_{i=0}^{l-1}$ can be obtained by the l-point IDFT of $\{\hat{H}_{im}\}_{i=0}^{l-1}$:

$$\hat{h}_i = \frac{1}{l} \sum_{k=0}^{l-1} \hat{H}_{km} W_l^{-ik}, \qquad 0 \leq i < l.$$

Once $\{\hat{h}_i\}_{i=0}^{l-1}$ are obtained, the channel frequency response can be estimated as N-point DFT

of the channel estimate $\hat{h}_i$ as follows:

$$\hat{H}_k = \frac{1}{N}\sum_{k=0}^{N-1} \hat{h}_i W_N^{ik}, \qquad 0 \le k < N.$$

The received data can be first estimated via

$$\hat{S}_k = \frac{Y_k}{\hat{H}_k}, \quad k = 0, 1, \cdots, N-1,$$

for those with index k not being a multiple of m and then detected by some quantization scheme dependent on the prior probability of the subcarriers.

It needs to be commented that in calculating M-point DFT or IDFT using Matlab command "fft" or "ifft", respectively, we need to multiply $1/\sqrt{M}$ for M-point DFT, and $\sqrt{M}$ for M-point IDFT, in order to be consistent with the DFT matrix and IDFT matrix used in OFDM.

3.2 Simulation Studies

In our simulation studies, the number of subcarriers N is 64, the length of cyclic-prefix l is 4, and the number of ensembles M is 20,000. We assume wide-sense stationary and uncorrelated scattering (WSSUS) channels, i.e., $\{h_i(k)\}_{i=0}^{l-1}$ are uncorrelated and are WSS process. However $h_i(k)$ changes slowly for each i, and hence, can be regarded as a time-invariant in each OFDM block.

To set up a Rayleigh fading channel for multipath propagation, we define a channel decay rate through defining $\sigma_{h_i}^2$, the mean power of $\{|h_i|\}$ as

$$\sigma_{h_{i+1}} = \frac{1}{2}\sigma_{h_i}, \qquad 0 \le i < l-1,$$

with a normalization of $\sigma_{h_0}^2 + \sigma_{h_1}^2 + \cdots + \sigma_{h_{l-1}}^2 = 1$. It should be clear that the exponential decay of the mean power does not necessarily mean $|h_i| > |h_{i+1}|$ for each i.

The N tones are assumed to have 4-QAM for their constellation. That is, each transmitted subcarrier has one value among $\{1, -1, j, -j\}$ in the frequency domain. In the receiver site, we need to detect each estimated data based on the constellation diagram via some quantization scheme. Assume that $S_k \in \{1, -1, j, -j\}$ has equal probability. Then the optimal detection yields the estimate $\hat{S}_k$ given by

$$\breve{S}_k = \begin{cases} 1, & \text{if } |\angle \hat{S}_k| < \frac{\pi}{4} \\ -1, & \text{if } |\angle \hat{S}_k| > \frac{3\pi}{4} \\ j, & \text{if } \frac{\pi}{4} < \angle \hat{S}_k < \frac{3\pi}{4} \\ -j, & \text{if } -\frac{3\pi}{4} < \angle \hat{S}_k < -\frac{\pi}{4} \end{cases}$$

where $\angle\theta$ has a range of $[-\pi,\ \pi]$ using the Matlab command "angle." Basically, the complex plane is divided into four sector regions with equal angle spans.

An efficient way is developed to carry out the detection algorithm in our simulation program, which is not described here. Let the number of ensembles be $M >> N$. The detection error rate is computed by counting the number of $\left|S_k - \breve{S}_k\right| > 1$, divided by M. The channel estimation error is assessed by computing root mean squared error (RMSE) given by

$$\text{RMSE} := \sqrt{\frac{1}{L_N} \sum_{k=1}^{L_N} \sum_{i=0}^{l-1} \left| h_i^{(k)} - \hat{h}_i^{(k)} \right|^2}.$$

To study the performance of the channel estimation and symbol detection, we used various values of signal-to-noise ratio (SNR) that are 10, 15, 20, 25, 30, 35, 40, 45, and 50 in our simulation study. The SNR is defined by

$$\text{SNR} = 10 \log \frac{\sigma_s^2}{\sigma_v^2} = 10 \log \frac{1}{\sigma_v^2},$$

if the subcarrier mean power is normalized to 1. Table 3.1 below shows the simulation result with their numerical values. Both the symbol detection error rate and channel estimate error

Table 3.1 The symbol detection error rate and the channel estimate error

SNR	10	15	20	25	30	35	40	45	50
Symbol error rate	0.0796	0.0232	0.0069	0.0021	0.0006	0.0002	7.1e-05	2.1e-05	4.6e-06
Channel error (RMSE)	0.3146	0.1782	0.1001	0.0563	0.0316	0.0178	0.0100	0.0056	0.0032

decrease as SNR increases. Note that channel coding is not employed and thus both errors are relatively larger than the practical WiFi results.

Figures 3.1 and 3.2 show the graphical results of the symbol detection error rate and RMSE of the channel estimation error, respectively. The symbol detection error rate shows from 0.0796 to 4.6e-06 according to SNR changes 10 to 50, respectively, with 20,000 ensembles. Under the same condition, RMSE of the channel estimation error ranges from 0.3146 to 0.0032.

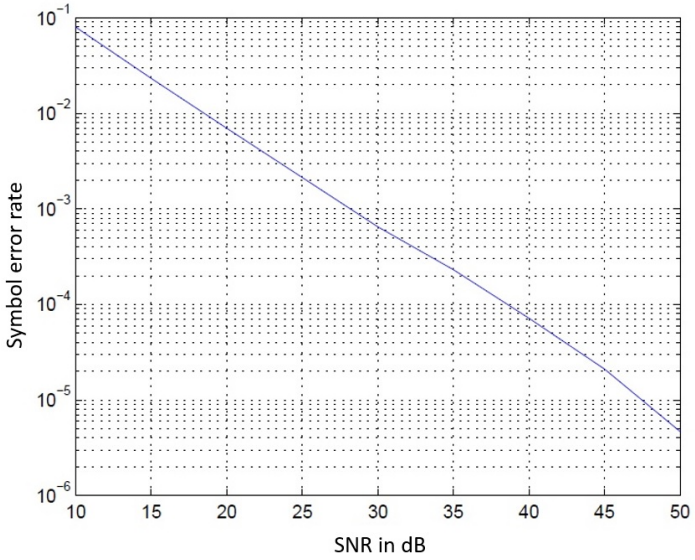

Figure 3.1 Symbol detection error rate

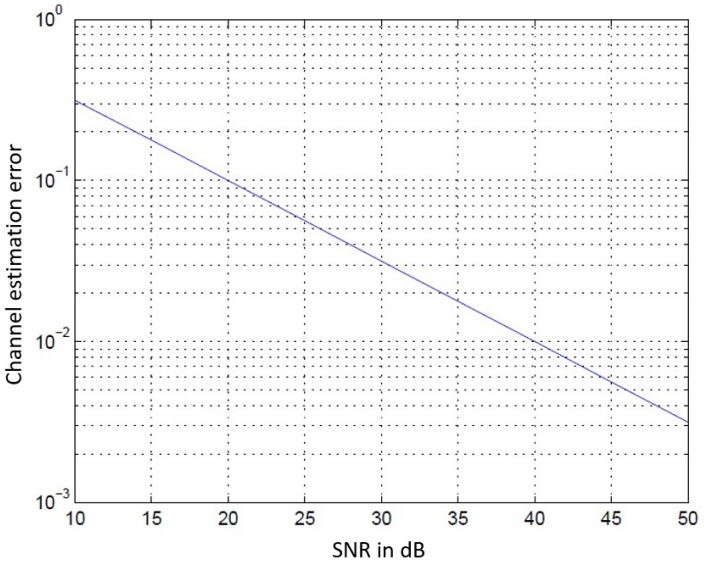

Figure 3.2 Channel estimation error

The result of this simulation shows acceptable error rates in both the symbol detection and channel estimation. So, it is expected that this can be applied to the TDOA estimate and localization purpose in the latter chapters.

3.3 Channel Estimation using the Kalman Filter

3.3.1 WSSUS Channel

The WSSUS channel is described as

$$h_i(k+1) = \alpha_i h_i(k) + \beta_i w_i(k)$$

for $0 \leq i < L$, where $w_i(k)$ is AWGN, satisfying $\mathrm{E}[w_i(k)] = 0, \mathrm{E}[w_i(k)^2] = 1$ and $|\alpha_i|^2 + |\beta_i|^2 = 1$. Let h and w be column vectors consisting of h_i and w_i at its $(i+1)$th entry, respectively. Then $h(k+1)$ can be described by

$$h(k+1) = \mathrm{diag}(\alpha_0, \cdots, \alpha_{L-1})h(k) + \mathrm{diag}(\beta_0, \cdots, \beta_{L-1})w(k).$$

In Matlab language, the initial value of $h(k)$ is taken to be

$$h(0) = (\mathrm{randn}(L,1) .* ah) + j(\mathrm{randn}(L,1) .* ah)$$

with $ah = [\ 5;\ 2.5;\ 1.25;\ 0.625\ ]$ for the case $L = 4$. In addition, $\alpha_i = 0.99$ and $\beta_i = \sqrt{1-\alpha_i^2}$ are set.

3.3.2 Channel Estimate at the First Block ($k = 0$)

Assuming that the entire block of OFDM symbol is used to estimate the channel at time $k = 0$. Then an optimal estimate of $h_i(0)$ based on the first block of $N = 64$ symbols can be taken as an MLE. Recall that $Y_i = H_i S_i + V_i = S_i H_i + V_i$. Packing together for $0 \leq i < N$

yields

$$Y := \begin{bmatrix} Y_0 \\ \vdots \\ Y_{N-1} \end{bmatrix} = \begin{bmatrix} S_0 & & \\ & \ddots & \\ & & S_{N-1} \end{bmatrix} \begin{bmatrix} H_0 \\ \vdots \\ H_{N-1} \end{bmatrix} + \begin{bmatrix} V_0 \\ \vdots \\ V_{N-1} \end{bmatrix} = C_0 h + V$$

Once C_0 is available, we can obtain the initial channel estimate via the MLE solution.

$$C_0 = \begin{bmatrix} S_0 & & \\ & \ddots & \\ & & S_{N-1} \end{bmatrix} \sqrt{N} F_{N,L}, \qquad W_N = e^{-j2\pi/N},$$

$$F_{N,L} = \frac{1}{\sqrt{N}} \begin{bmatrix} 1 & 1 & 1 & \cdots & 1 \\ 1 & W_N^1 & W_N^2 & \cdots & W_N^{L-1} \\ \vdots & \vdots & \vdots & \cdots & \vdots \\ 1 & W_N^{N-1} & W_N^{2(N-1)} & \cdots & W_N^{(L-1)(N-1)} \end{bmatrix}$$

The aforementioned assumption leads to

$$\hat{h}_{0|0} := \theta_{\text{MLE}} = (C_0' {\Sigma_v}^{-1} C_0)^{-1} C_0' {\Sigma_v}^{-1} Y = C_0' Y / N \quad (\because (C_0' C_0)^{-1} = 1/N),$$
$$\Sigma_{0|0} = \text{cov}[\hat{h}_{0|0}] = (C_0' {\Sigma_v}^{-1} C_0)^{-1}$$

where the covariance $\Sigma_v = \text{diag}(\sigma_{v_0}^2, \cdots, \sigma_{v_{N-1}}^2)$. In Matlab language, $Y = fft(y)/\sqrt{N}$.

3.3.3 Channel Estimate from Later Blocks ($k \geq 1$)

We use Kalman filter to estimate $\{h_i(k)\}_{i=0}^{L-1}$ for $k = 1, 2, \cdots$, based on the initial estimate and pilot tones at each block of the OFDM symbol. Let

$$A = \text{diag}(\alpha_0, \cdots, \alpha_{L-1}), \qquad B = \text{diag}(\beta_0, \cdots, \beta_{L-1}).$$

By taking $x(k) = h(k)$, we have the following state space model:

$$x(k+1) = Ax(k) + Bw(k), \qquad y(k) = C_k x(k) + v(k).$$

The measurement equation is more tricky, because only L pilot symbols can be used in the measurement equation for $y(k)$ that can be written as

$$y(k) = \begin{bmatrix} Y_0(k) \\ Y_m(k) \\ \vdots \\ Y_{(L-1)m}(k) \end{bmatrix} = \begin{bmatrix} S_0(k) & & & \\ & S_m(k) & & \\ & & \ddots & \\ & & & S_{(L-1)m}(k) \end{bmatrix} \sqrt{L} F_L \begin{bmatrix} h_0(k) \\ \vdots \\ h_{L-1}(k) \end{bmatrix} + \begin{bmatrix} V_0(k) \\ V_m(k) \\ \vdots \\ V_{(L-1)m}(k) \end{bmatrix},$$

by taking $m = N/L$, is assumed to be an integer. Recall the expression of the DFT matrix $F_{N,L}$ in the previous page. So $F_L = F_{L,L}$ is the same as $F_{N,L}$ except that N is replaced by L. It follows

$$C_k = \begin{bmatrix} S_0(k) & & & \\ & S_m(k) & & \\ & & \ddots & \\ & & & S_{(L-1)m}(k) \end{bmatrix} \sqrt{L} F_L, \quad F_L = \tfrac{1}{\sqrt{L}} \begin{bmatrix} 1 & 1 & 1 & \cdots & 1 \\ 1 & W_L & W_L^L & \cdots & W_L^{L-1} \\ \vdots & \vdots & \vdots & \cdots & \vdots \\ 1 & W_L^{L-1} & W_L^{2(L-1)} & \cdots & W_L^{(L-1)^2} \end{bmatrix}.$$

The Kalman filter can be used to estimate $h(k) = x(k)$ in accordance with

$$\hat{x}_{k|k} = (I + L_k C_k)\hat{x}_{k|k-1} - L_k y(k)$$

initialized by $\hat{x}_{1|0} = A\hat{h}_{0|0}$ with an error covariance of $\Sigma_{1|0} = A\Sigma_{0|0}A^* + BB^*$, where $L_k = -\Sigma_k C_k^* (R_k + C_k \Sigma_k C_k^*)^{-1}$,

$$R_k = \mathrm{E}[v(k)v(k)^*] = \mathrm{diag}(\sigma_{v_0}^2, \cdots, \sigma_{v_{(L-1)m}}^2)$$

is diagonal of dimension $L \times L$, and the error covariance for $\hat{x}_{k|k}$ is given by

$$\Sigma_{k|k} = \text{cov}[\hat{x}_{k|k}] = \Sigma_k - \Sigma_k C_k^*(R_k + C_k \Sigma_k C_k^*)^{-1} C_k \Sigma_k.$$

The predicted channel is

$$\hat{x}_{k+1|k} = A\hat{x}_{k|k}$$

with the prediction error covariance

$$\Sigma_{k+1|k} = A\Sigma_k A^* + BB^* - A\Sigma_k C_k^*(R_k + C_k \Sigma_k C_k^*)^{-1} C_k \Sigma_k A^* = A\Sigma_{k|k} A^* + BB^*$$

3.3.4 Simulation Results

Table 3.2 shows the simulation results with their numerical values when the Kalman filter is used. Both the symbol detection error rate and channel estimation error decrease as the SNR increases, as in the previous algorithm. The symbol detection error rates are from 3.35% to 4.7e-06% according to the SNR changes 10 to 50, respectively, with 20,000 ensembles. The RMSE of the channel estimation error ranges from 0.2404 to 0.0032. Figures 3.3 and 3.4 show the graphical results when the Kalman filter is used.

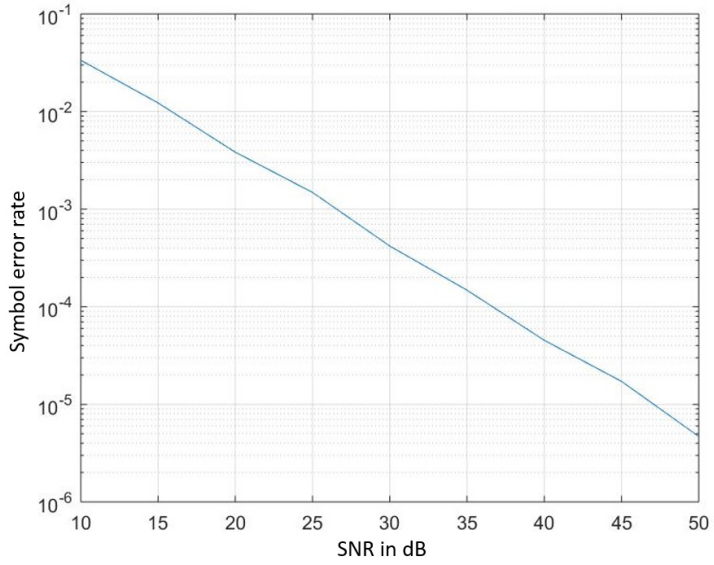

Figure 3.3 Symbol detection error rate using the Kalman filter

Table 3.2 The symbol detection error rate and channel estimate error using the Kalman filter

SNR	10	15	20	25	30	35	40	45	50
Symbol error rate (%)	3.35	1.23	0.38	0.15	0.0419	0.0148	4.5e-03	1.7e-03	4.7e-06
Channel error (RMSE)	0.2404	0.1559	0.0947	0.0552	0.0314	0.0178	0.0100	0.0056	0.0032

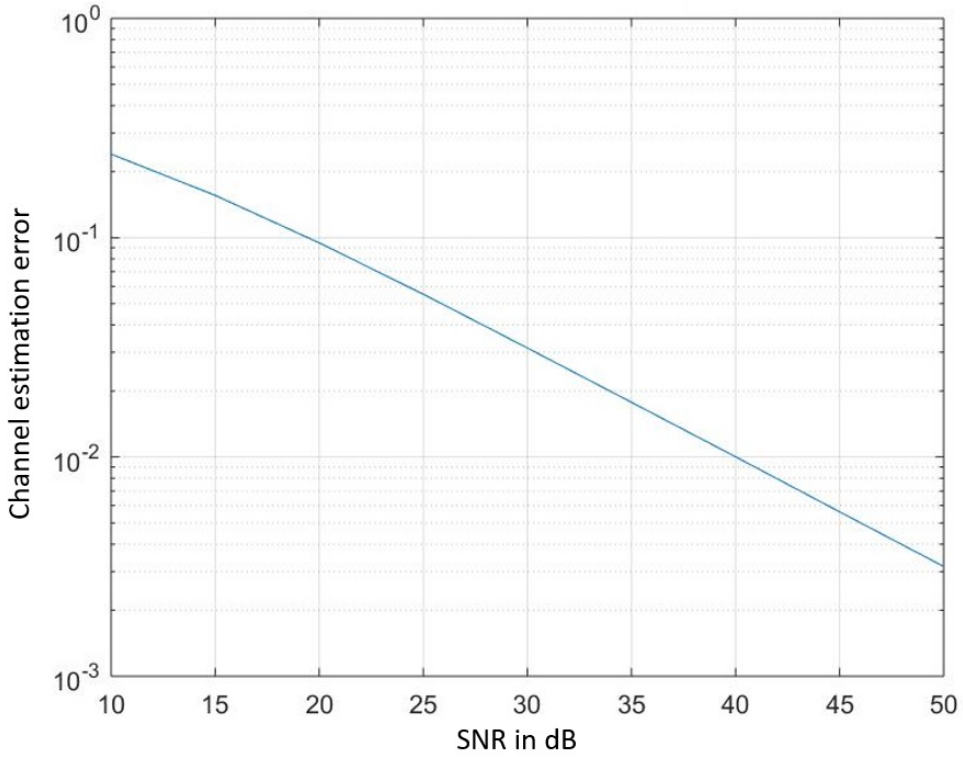

Figure 3.4 Channel estimation error using the Kalman filter

Table 3.3 shows the performance improvement rate when we use the Kalman filter for the symbol detection and channel estimation compared to the first one that we used in this chapter. That is, it shows how much the symbol error rate and the channel estimation error have decreased. For example, when the SNR is 10, the symbol error rate and the channel estimation error decreased by 4.61% and 0.0742, respectively. As the results show, when the Kalman filter is applied, the performance improved more in the lower SNR and there was not much of a difference in the performance as the SNR increased.

Table 3.3 Performance improvement rate using the Kalman filter

SNR	10	15	20	25	30	35	40	45	50
Symbol error rate (%)	4.61	1.09	0.31	0.06	0.02	0.01	2.6e-05	4e-06	4.55e-06
Channel error (RMSE)	0.0742	0.0223	0.0054	0.0011	0.0002	0	0	0	0

CHAPTER 4
TDOA ESTIMATION

This chapter summarizes the TDOA estimation procedure and simulation results.

4.1 TDOA Estimation Procedure

TDOA is defined as the difference between the time from the mobile target to the first sensor and the target to the second sensor, if we assume there are two sensors as it is shown in Figure 4.1.

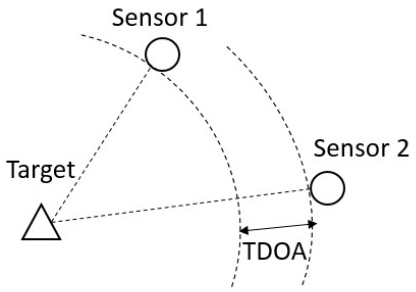

Figure 4.1 Schematic illustration of TDOA

In order to estimate TDOA for localization purposes, we used the procedure in Figure 4.2.

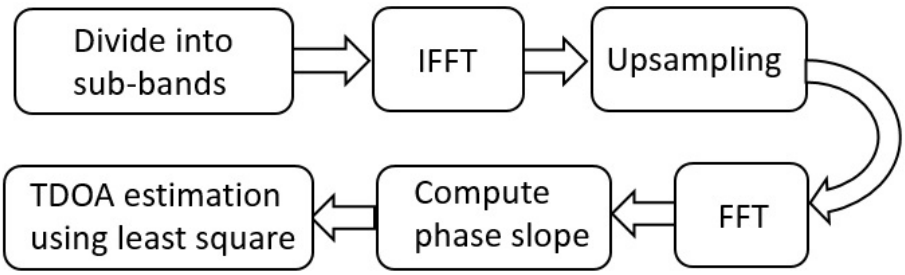

Figure 4.2 Block diagram of the TDOA estimation procedure

As discussed in Chapter 3, we divide each OFDM symbol into 8 subbands. The sensors receive the OFDM symbols in the frequency domain. Figure 4.3 shows how to do sub-band division.

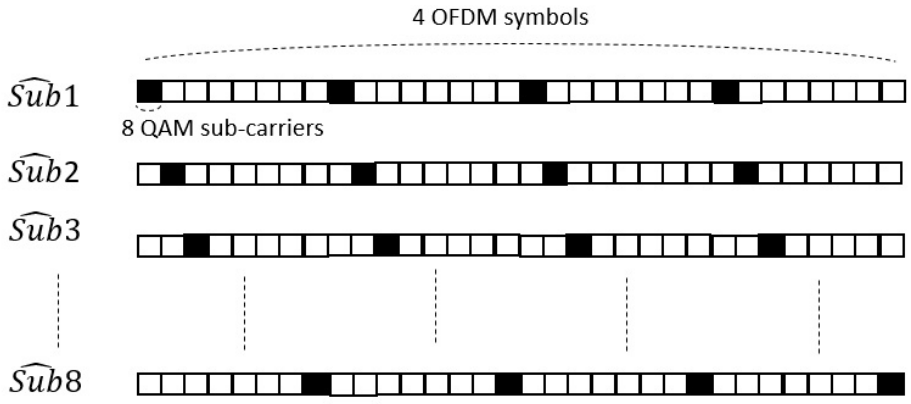

Figure 4.3 Sub-band division

Let $\{\hat{sub}_i\}_{i=1}^{L}$ be the sub-bands of each sensor in the frequency domain, where L is the number of the sub-band. In Figure 4.3, each box represents 8 QAM sub-carriers and every 8 boxes represent one OFDM symbol. In every OFDM symbol, the first 8 QAM subcarriers from the original received data are placed in $\hat{sub}_1$. The rest of the OFDM symbol has zero padding. We can obtain $\hat{sub}_2$ to $\hat{sub}_8$ in a similar way, except that they are each placed 8 QAM sub-carriers later. Then we use inverse DFT to convert these eight sub-bands into the time domain. In the time domain, each sub-band signal is denoted by $\{sub_i\}_{i=1}^{L}$ as follows:

$$\begin{array}{ccc} \hat{sub}_1 & & sub_1 \\ \hat{sub}_2 & IDFT & sub_2 \\ \vdots & \Longrightarrow & \vdots \\ \hat{sub}_8 & & sub_8 \end{array} .$$

Then, we do upsampling to increase the sampling frequency so that we can compute the TDOA more accurately. Figure 4.4 shows the received sub-band signals from two different sensors in the time domain. Recall TDOA is induced by the difference in distance. In Figure 4.4, sensor 1 is closer to the target than sensor 2, and TDOA is proportional to the distance difference. In the simulation studies, TDOA needs to be added in accordance with the difference in distance.

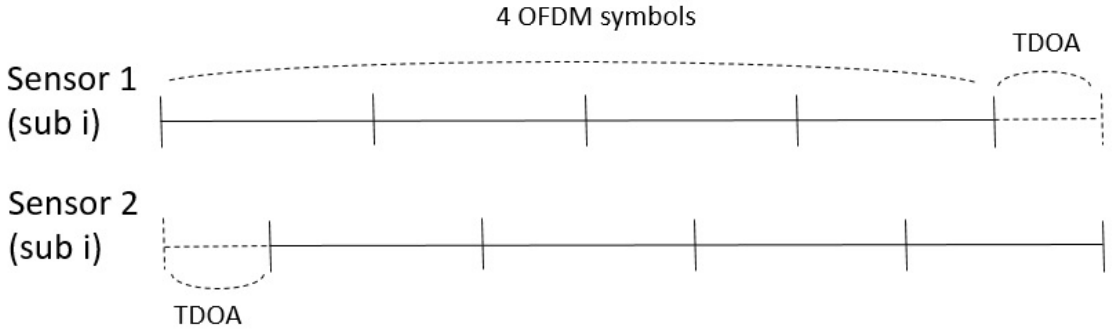

Figure 4.4 Received sub-band signals showing TDOA

Let k be an integer-valued time index, and $\{s_{1i}(k)\}$ and $\{s_{2i}(k)\}$ be sampled signals of the same continuous-time signal received at the ith sub-band of sensor 1 and ith sub-band of sensor 2, respectively. Then $\{S_{1i}(\Omega)\}$ and $\{S_{2i}(\Omega)\}$ are the DFT of $\{s_{1i}(k)\}$ and $\{s_{2i}(k)\}$. There holds $S_{2i}(\Omega) = e^{j\Omega\Delta t}S_{1i}(\Omega)$ where Δt is the TDOA. Thus we can compute the TDOA by the phase slope, that is, $\angle S_{1i}(e^{jw_k})^* S_{2i}(e^{jw_k})$ where $w_k = \frac{(k-1)2\pi}{N_T}$, $k = 1, 2, \cdots, N_T$. In general, note that $N_T \neq N$.

In order to find the phase slope, we used the least square method. Let $aw_k + b$ be the slope. Then the least square is written as follows:

$$\sum_{k=0}^{N-1} |\angle S_{1i}(e^{jw_k})^* S_{2i}(e^{jw_k}) - (aw_k + b)|^2, \quad w_k = \frac{(k-1)2\pi}{N_T}, \quad k = 1, 2, \cdots, N_T. \tag{4.1}$$

Let $Y_l(w_k)$ be $S_1(e^{jw_k})^* S_l(e^{jw_k})$. Then 4.1 is re-written as:

$$\sum_{k=0}^{N_T-1} |Y_l(w_k) - (aw_k + b)|^2 = \sum_{k=0}^{N_T-1} \left| Y_l(w_k) - [w_k \;\; 1] \begin{bmatrix} a \\ b \end{bmatrix} \right|^2 \tag{4.2}$$

$$= \sum_{k=0}^{N-1} \left| \begin{bmatrix} Y(w_1) \\ \vdots \\ Y(w_{N_T}) \end{bmatrix} - \begin{bmatrix} w_1 & 1 \\ \vdots & \\ w_{N_T} & 1 \end{bmatrix} \begin{bmatrix} a \\ b \end{bmatrix} \right|^2 \tag{4.3}$$

Let $A = [w_k \;\; 1]$, $X = \begin{bmatrix} a \\ b \end{bmatrix}$. Then the equation to minimize 4.2 is given by

$$||Y - AX||^2.$$

Then we can find the optimal value of X by using the least square method as shown below:

$$X_{opt} = (A'A)^{-1}A'Y = \begin{bmatrix} a_{opt} \\ b_{opt} \end{bmatrix}.$$

The estimated TDOA of ith sub-band is

$$\hat{TDOA}_i = a_{opt}T_s$$

where T_s is the sampling period. Finally, the mean value of $\{\hat{TDOA}_i\}_{i=1}^{L}$ would be the optimal estimate TDOA as follows:

$$\hat{TDOA} = \frac{1}{L}\sum_{i=1}^{L}\hat{TDOA}_i.$$

4.2 Simulation Studies

In these simulation studies, we used 7 sensors. The target is located at (110, 45,1) on the x-y-z plane. The sensors' locations can be seen in Figure 4.5. We assumed that the SNR is 20 dB. According to the symbol detection simulation in Chapter 3, we used the symbol error rate of 0.0069. Figure 4.6 shows an example of the phase slope plot. In this example, the phase was computed by sensor 1 and sensor 3. Each sub-band shows a slightly different slope due to probably the data detection error and channel estimation error. Recall that a SNR of 20 dB involves a significant detection error rate. Hence, we use the average as the final estimated TDOA value.

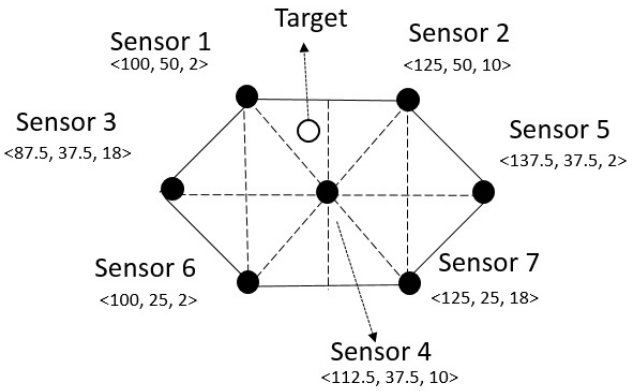

Figure 4.5 Location of the target and sensors

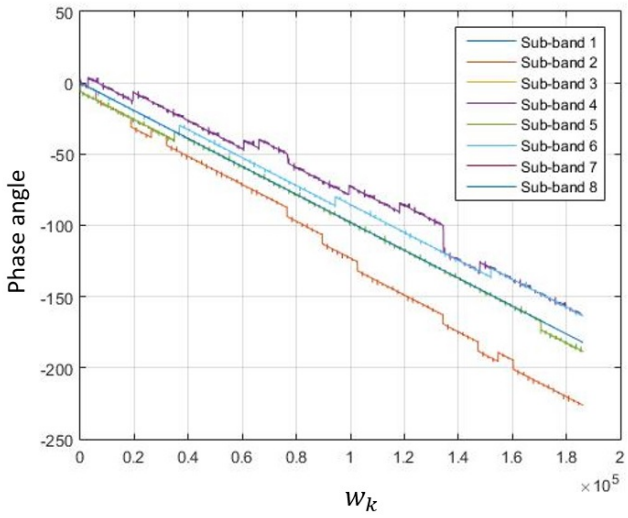

Figure 4.6 An example of the phase slope plot

When we set the first sensor as the origin, 6 pairs of sensors are formed. That is, <sensor 1 and sensor 2>,<sensor 1 and sensor 3>, $\cdots$, <sensor 1 and sensor 7>. The received sub-band signal in the time domain at each sensor is upsampled by a factor of 25 and a total of 200 ensembles are simulated. Table 4.1 shows the true TDOA values at each paired sensor, mean of estimated TDOA, and the standard deviation. The numbers in the first row indicate the sensor pairs <sensor 1 and sensor 2>, $\cdots$, <sensor 1 and sensor 7>.

Table 4.1 TDOA estimation results with a SNR of 20 dB

	1 & 2	1 & 3	1 & 4	1 & 5	1 & 6	1 & 7
True TDOA (ns)	23.23	59.85	2.51	57.66	37.19	63.36
Mean of TDOA estimate (ns)	18.45	58.77	2.29	54.15	32.71	60.84
SD (ns)	44.06	40.42	46.28	41.84	56.76	41.43

Table 4.2 shows the TDOA estimation results with a SNR of 50 dB. It was simulated with 2000 ensembles in order to get more accurate results because it has a very small data detection error. As seen in the results, the mean of the TDOA estimate is closer to the true TDOAs and they have smaller standard deviations.

Table 4.2 TDOA estimation results with a SNR of 50 dB

	1 & 2	1 & 3	1 & 4	1 & 5	1 & 6	1 & 7
Mean of TDOA estimate (ns)	22.00	58.00	2.00	55.91	35.98	62.00
SD (ns)	21.89	4.69	0.79	20.67	15.84	4.02

Overall, the estimated TDOA is very close to the true TDOA. The standard deviation is also small and thus this TDOA estimation algorithm performs quite well.

CHAPTER 5
LOCALIZATION

5.1 Problem Formulation and Preliminary Analysis

Denote (x_k, y_k, z_k) as the position of the kth sensor and (x_T, y_T, z_T) as the position of the stationary target. Our goal is to estimate the position (x_T, y_T, z_T) based on the L TDOA estimates collected by each of the n sensors located at $\{(x_k, y_k, z_k)\}_{k=1}^n$. Let

$$R_{k,T} = \sqrt{(x_T - x_k)^2 + (y_T - y_k)^2 + (z_T - z_k)^2}$$

be the distance between the target and the kth sensor. By an abuse of notation, $R_T = R_{1,T}$. Basically, the position of the first sensor is treated as the origin of the Cartesian coordinate system. Then the TDOA between the kth and first sensor for receiving the RF signal from the target is defined as

$$\Delta t_k := [R_{k,T} - R_T]/c \tag{5.1}$$

for k =2, 3, $\cdots$, n with c as the speed of light. The target location is embedded in TDOAs or $\Delta t_k = \Delta t_k(x_T, y_T, z_T)$. As in the literature we assume that the estimates of the TDOAs are given by

$$\Delta \hat{t}_{k;i} = \Delta t_k(x_T, y_T, z_T) + \delta t_{k;i} \tag{5.2}$$

for i=1, 2, $\cdots$, L where $\{\delta t_{k;i}\}_{k=2}^n$ are uncorrelated Gaussian random variables with mean zero and variance σ_k^2. That is, the measurement noises have the joint probability density function (PDF) of

$$p_\Delta(\delta t | x_T, y_T, z_T) = \frac{1}{\sqrt{(2\pi)^{L(n-1)}}\sigma_k^{L(n-1)}} \exp\left\{ -\sum_{i=1}^{L}\sum_{k=2}^{n} \frac{[\Delta \hat{t}_{k;i} - \Delta t_k(x_T, y_T, z_T)]^2}{2\sigma_k^2} \right\}. \tag{5.3}$$

It follows that source localization based on TDOAs is a nonlinear estimation problem. Denote $\rho_k = \sqrt{x_k^2 + y_k^2 + z_k^2}$ for $1 \leq k \leq n$, and rewrite (5.1) equivalently as

$$(x_T - x_k)^2 + (y_T - y_k)^2 + (z_T - z_k)^2 = (\sqrt{(x_T - x_k)^2 + (y_T - y_k)^2 + (z_T - z_k)^2} + c\Delta t_k)^2.$$

The above can be written equivalently in the following equation:

$$\rho_k^2 - \rho_1^2 = 2[(x_k - x_1)x_T + (y_k - y_1)y_T + (z_k - z_1)z_T] + c^2\Delta t_k^2 + 2cR_T\Delta t_k$$

for $2 \leq k \leq n$. The TDOA data in (5.2) can be substituted in to obtain a quasi-linear model [4], [7], [16], [17]. Indeed denote

$$a_{k;i} = \rho_k^2 - \rho_1^2 - c^2(\Delta\hat{t}_{k;i}^2 + \mu\sigma_k^2), \;\; \eta_{k;i} = -2c(R_T + c\Delta\hat{t}_{k;i})\delta t_{k;i} + c^2(\delta t_{k;i}^2 - \mu\sigma_k^2) \qquad (5.4)$$

for $2 \leq k \leq n$ and $1 \leq i \leq L$ where $\mu \geq 0$. Let $\theta = [\; x_T \;\; y_T \;\; z_T \;\; R_T \;]'$ be the location parameter vector to be estimated. The quasi-linear model $\underline{a} = H\theta + \underline{\eta}$ holds. That is,

$$\begin{bmatrix} \underline{a}_2 \\ \underline{a}_3 \\ \vdots \\ \underline{a}_n \end{bmatrix} = 2 \begin{bmatrix} x_{2,1}\mathbf{1}_L & y_{2,1}\mathbf{1}_L & z_{2,1}\mathbf{1}_L & c\Delta\hat{\underline{t}}_2 \\ x_{3,1}\mathbf{1}_L & y_{3,1}\mathbf{1}_L & z_{3,1}\mathbf{1}_L & c\Delta\hat{\underline{t}}_3 \\ \vdots & \vdots & \vdots & \vdots \\ x_{n,1}\mathbf{1}_L & y_{n,1}\mathbf{1}_L & z_{n,1}\mathbf{1}_L & c\Delta\hat{\underline{t}}_n \end{bmatrix} \begin{bmatrix} x_T \\ y_T \\ z_T \\ R_T \end{bmatrix} + \begin{bmatrix} \underline{\eta}_2 \\ \underline{\eta}_3 \\ \vdots \\ \underline{\eta}_n \end{bmatrix} \qquad (5.5)$$

where $\mathbf{1}_L$ is an L-dimensional vector of 1s and

$$\underline{a}_k = \begin{bmatrix} a_{k;1} \\ \vdots \\ a_{k;L} \end{bmatrix}, \;\; \Delta\hat{\underline{t}}_k = \begin{bmatrix} \Delta\hat{t}_{k;1} \\ \vdots \\ \Delta\hat{t}_{k;L} \end{bmatrix}, \;\; \underline{\eta}_k = \begin{bmatrix} \eta_{k;1} \\ \vdots \\ \eta_{k;L} \end{bmatrix}, \;\; \begin{bmatrix} x_{k,1} \\ y_{k,1} \\ z_{k,1} \end{bmatrix} = \begin{bmatrix} x_k - x_1 \\ y_k - y_1 \\ z_k - z_1 \end{bmatrix}$$

for $2 \leq k \leq n$. Equation (5.5) is the same as the quasi-linear model in the literature except a multiple of TDOA estimates at each sensor with $\{a_{k;i}\}$ pseudo-measurements and $\{\eta_{k;i}\}$ the

corresponding noises. However, it imposes a constraint to the parameter vector θ as

$$(\theta - \theta_0)'Q(\theta - \theta_0) = 0, \quad Q = diag(1, 1, 1, -1) \tag{5.6}$$

where $\theta_0 = [\ x_1 \ \ y_1 \ \ z_1 \ \ 0\ ]'$, that is a zero vector, if the sensor node 1 is treated as the origin. Denote $\mathrm{E}\{\cdot\}$ and $\mathrm{E}\{\cdot|\cdot\}$ as the expectation and conditional expectation. When μ=1,

$$E\{\eta_{k;i}|\Delta\hat{t}_{k;i}\} = 0, \quad E\{\eta_{k;i}^2|\Delta\hat{t}_{k;i}\} = 4c^2(R_T + c\Delta\hat{t}_{k;i})^2\sigma_k^2 + 2c^4\sigma_k^4 \tag{5.7}$$

where $\mathrm{E}\{\delta t_{k;i}^3\}$=0 and $\mathrm{E}\{\delta t_{k;i}^4\} = 3\sigma_k^4$ are used. The equation is under condition $\{\eta_{k;i}\}$, which are Gauss distributed, assuming that $\{\delta t_{k;i}\}$ are Gauss distributed with zero mean. The next lemma is useful.

Lemma 1. Let V be Gauss distributed with mean zero and variance σ^2. If the ratio of $\gamma > 0$ to σ is suitably large, e.g., greater than 10, then $\Xi = -2\gamma V + V^2$ is a good approximation to the Gauss random variable of mean 0 and variance $4\gamma^2\sigma^2$.

It can be easily seen that $\Xi = \eta_{k;i}$ has the same form as in Lemma 1 by taking $\mu = 0, \sigma = c\sigma_k$, and by (5.1),

$$\gamma = \gamma_{k;i} := R_T + c\Delta\hat{t}_{k;i} \approx R_{x,T} \tag{5.8}$$

for each k. Hence, the assumption on the large ratio of γ to σ holds approximately, if

$$\frac{\gamma}{\sigma} = \frac{R_T + c\Delta\hat{t}_{k;i}}{c\sigma_k} \approx \frac{R_{k,T}}{c\sigma_k} >> 1 \ \ \forall \ \ k, \tag{5.9}$$

which holds generically. The reason lies in the fact that $c\sigma_k$ represents the resolution of the TDOA estimates in terms of the distance while $R_{k,T}$ is the distance between the kth sensor and the target. For this reason (5.9) holds true unless in some very special situations (that cab ne removed by deleting the sensor too close to that target). As such, $\{\eta_{k;i}\}$ are approximately Gauss distributed with mean zero and variance $\{\gamma_{i,k}^2\sigma_k^2\}$ in the case of μ=0.

The joint PDF in (5.3) can be replaced by the following PDF

$$p\Xi(\eta; x_T, y_T, z_T) \approx \frac{1}{\sqrt{(2\pi)^{L(n-1)} det(\Sigma)}} \exp\big[-\frac{1}{2}(\underline{a} - H\theta)'\Sigma^{-1}(\underline{a} - H\theta)\big]. \tag{5.10}$$

Since the TDOA estimation errors are uncorrelated, the noise covariance matrix Σ is given by

$$\Sigma = 4c^2 \mathrm{diag}(\gamma_{2;1}^2\sigma_2^2, \cdots, \gamma_{2;\mathrm{L}}^2\sigma_2^2, \cdots, \gamma_{\mathrm{n};1}^2\sigma_{\mathrm{n}}^2, \cdots, \gamma_{\mathrm{n};\mathrm{L}}^2\sigma_{\mathrm{n}}^2). \tag{5.11}$$

Recall the constraint (5.6) for the parameter vector. Hence, an approximate MLE for the location parameter vector θ is the one that minimizes

$$J = \frac{1}{2}(\underline{a} - H\theta)'\Sigma^{-1}(\underline{a} - H\theta), \tag{5.12}$$

which is subject to the constraint (5.6) under the condition (5.9). A solution will be provided in the next section to such constrained WLS problems. We provide an approximate expression for the Fisher information matrix (FIM) associated with the quasi-linear model (5.5).

Lemma 2. If the noise vector in the quasi-linear model (5.5) admits an approximate joint PDF in (5.10), then the associated FIM with respect to the location parameter (x_T, y_T, z_T) is approximately given by

$$FIM \approx (H_1 + \underline{b}v'_{\alpha,\beta})'\Sigma^{-1}(H_1 + \underline{b}v'_{\alpha,\beta}), \tag{5.13}$$

where $z_T - z_1 = R_T \cos\alpha$, $y_T - y_1 = R_T \sin\alpha\cos\beta$, $x_T - x_1 = R_T \sin\alpha\sin\beta$, and

$$v_{\alpha,\beta} = \begin{bmatrix} \sin\alpha\sin\beta \\ \sin\alpha\cos\beta \\ \cos\alpha \end{bmatrix}, \quad H_1 = \begin{bmatrix} x_{2,1}\mathbf{1}_L & y_{2,1}\mathbf{1}_L & z_{2,1}\mathbf{1}_L \\ x_{3,1}\mathbf{1}_L & y_{3,1}\mathbf{1}_L & z_{3,1}\mathbf{1}_L \\ \vdots & \vdots & \vdots \\ x_{n,1}\mathbf{1}_L & y_{n,1}\mathbf{1}_L & z_{n,1}\mathbf{1}_L \end{bmatrix}, \quad \underline{b} = \begin{bmatrix} c\Delta\hat{\underline{t}}_2 \\ c\Delta\hat{\underline{t}}_3 \\ \vdots \\ c\Delta\hat{\underline{t}}_n \end{bmatrix}.$$

That is, β is the bearing parameter on the $x-y$ plane, α is the angle between the positive z-axis and $x-y$ plane, and $H = [\ H_1\ \ \underline{b}\ ]$.

5.2 Solution to the Constrained WLS Problem

Minimization of J in (5.12) subject to the constraint (5.6) has been tackled in [7], [17], [18] and in [4], [11]. Several solution procedures have been developed, but they all bypass the difficulty in solving the constrained WLS problem directly. In this section, we provide a general solution to

$$\min_{\theta' Q \theta = 0} \frac{1}{2}(\underline{a} - H\theta)' \Sigma^{-1} (\underline{a} - H\theta). \tag{5.14}$$

The solution to the above constrained WLS is applicable to the case when the constraint is given by $(\theta - \theta_0)' Q (\theta - \theta_0) = 0$ with $\theta_0 \neq 0$. In (5.14), the matrix Q is an indefinite nonzero matrix with size $l \times l$ and matrix H has rank l, which is its number of columns. For its application to our localization problem, l=4.

We employ the method of the Lagrange multiplier to solve (5.14). Let λ be real and consider

$$J = \frac{1}{2}[(H\theta - \underline{a})' \Sigma^{-1} (H\theta - \underline{a}) + \lambda \theta' Q \theta]. \tag{5.15}$$

Then the necessary condition for optimality yields the condition

$$H' \Sigma^{-1} (H\theta - \underline{a}) + \lambda Q \theta = 0 \iff \theta = (H' \Sigma^{-1} H + \lambda Q)^{-1} H' \Sigma^{-1} \underline{a}. \tag{5.16}$$

An optimal solution needs to satisfy the constraint $\theta' Q \theta$=0 leading to

$$\underline{a}' \Sigma^{-1} H (H' \Sigma^{-1} H + \lambda Q)^{-1} Q (H' \Sigma^{-1} H + \lambda Q)^{-1} H' \Sigma^{-1} \underline{a} = 0. \tag{5.17}$$

The solution algorithm is hinged on the computation of the real root λ from the above equation and there can be more than one such real root. The result of simultaneous diagonalization in [10] can be employed for this purpose. Because $\Sigma = \Sigma' > 0$ and $Q = Q'$, there

exists an nonsingular matrix S, such that $H'\Sigma^{-1}H = SD_\Sigma S'$ and $Q = SD_Q S'$, where D_Σ and D_Q are both diagonal. It is noted that D_Σ and D_Q have the same inertia as Σ and Q, respectively. It follows that (5.17) is equivalent to

$$(S^{-1}H'\Sigma^{-1}\underline{a})'(\lambda I + D_\Sigma D_Q^{-1})^{-1}D_Q^{-1}(\lambda I + D_\Sigma D_Q^{-1})^{-1}(S^{-1}H'\Sigma^{-1}\underline{a}) = 0. \tag{5.18}$$

Let $D_Q^{-1} = diag(q_1, q_2, \cdots, q_l)$. Then it has the same number of negative and positive elements as $D = D_\Sigma D_Q^{-1} = diag(d_1, d_2, \cdots, d_l)$ by the positivity of Σ and D_Σ. In fact, $q_i d_i > 0$. The matrices S and D can be obtained by eigenvalue decomposition of $H'\Sigma^{-1}HQ^{-1} = SDS^{-1}$. Let v_i be the ith element of $S^{-1}H'\Sigma^{-1}\underline{a}$. Then (5.18) is equivalently converted into the following:

$$(S^{-1}H'\Sigma^{-1}\underline{a})'(\lambda I + D_Q^{-1}D_\Sigma)^{-1}D_Q^{-1}(\lambda I + D_\Sigma D_Q^{-1})^{-1}(S^{-1}H'\Sigma^{-1}\underline{a}) = \sum_{i=1}^{l}\frac{q_i v_i^2}{(\lambda + d_i)^2} = 0. \tag{5.19}$$

Because Q is indefinite, there is at least one strictly positive and one strictly negative element from $\{q_i\}_i^l = 1$. Hence, the above equation has at least one real root. However, there are only finitely many real λ values satisfying (5.19). In fact, all the roots of the nonlinear equation in (5.19) are roots of the following polynomial with degree $2(l-1)$:

$$\sum_{i=1}^{l} q_i v_i^2 \prod_{k\neq i}(\lambda + d_k)^2 = 0. \tag{5.20}$$

For source localization based on TDOAs, the constraint is given by (5.6) in which case l=4 implying that the computational complexity due to the roots computation is rather modest. Denote $\{\lambda_k\}_{k=1}^r$ as the r real roots of (5.20). Now by (5.16),

$$\begin{aligned} H\theta - \underline{a} &= [H(H'\Sigma^{-1}H + \lambda_k Q)^{-1}H'\Sigma^{-1} - I]\underline{a} \\ &= [HQ^{-1}(\lambda_k I + H'\Sigma^{-1}HQ^{-1})^{-1}H'\Sigma^{-1} - I]\underline{a} \\ &= [(\lambda_k I + HQ^{-1}H'\Sigma^{-1})^{-1}HQ^{-1}H'\Sigma^{-1} - I]\underline{a} \end{aligned}$$

$$= -\lambda_k(\lambda_k I + HQ^{-1}H'\Sigma^{-1})^{-1}\underline{a}$$
$$= -\lambda_k\Sigma(\lambda_k\Sigma + HQ^{-1}H')^{-1}\underline{a}.$$

Substituting the above into the performance index leads to

$$J = \frac{1}{2}\lambda_k^2\underline{a}'(\lambda_k\Sigma + HQ^{-1}H')^{-1}\Sigma(\lambda_k\Sigma + HQ^{-1}H')^{-1}\underline{a}. \tag{5.21}$$

Let λ_{opt} be one of the r real roots that minimizes J over $\{\lambda_k\}_{k=1}^r$. Then in light of (5.16), the optimal θ is obtained as $\theta = \theta_{opt}$ given by

$$\theta_{opt} = [H'\Sigma^{-1}H + \lambda_{opt}Q]^{-1}H'\Sigma^{-1}\underline{a}. \tag{5.22}$$

The above solution procedure is summarized into the following result.

Theorem 1. Consider the constrained WLS manifested as in (5.14). Let $H'\Sigma^{-1}HQ^{-1} = SDS^{-1}$ be the eigenvalue decomposition with $\{d_i\}$ eigenvalues. Then there hold

$$H'\Sigma^{-1}H = SD_\Sigma S', \;\; Q = SD_Q S', \tag{5.23}$$

with D_Σ and D_Q diagonal and $D = D_\Sigma D_Q^{-1}$. Denote $\underline{v} = S^{-1}H'\Sigma^{-1}\underline{a}$ and $\{\lambda_k\}$ as real roots of (5.20). If λ_{opt} minimizes J in (5.21) over $\{\lambda_k\}$, then the solution to the constrained WLS is given by (5.22).

Remark 1. If the quadratic constraint is $\delta\theta'Q\delta\theta = (\theta-\theta_0)'Q(\theta-\theta_0)$, which involves $\theta_0 \neq 0$, then by $H\theta = H\theta_0 + H\delta\theta$, we may consider solving it alternatively as

$$\min_{\delta\theta'Q\delta\theta=0} \frac{1}{2}[(\underline{a} - H\theta_0) - H\delta\theta]'\Sigma^{-1}[(\underline{a} - H\theta_0) - H\delta\theta].$$

The above is identical to the constrained WLS in (5.14) with $\delta\theta$ as unknown, to which the solution procedure developed prior to Theorem 1 is applicable. After the optimal $\delta\theta_{opt}$ is available, $\theta_{opt} = \delta\theta_{opt} + \theta_0$ can also be obtained.

It is noted that in applying the solution procedure in Theorem 1 to source localization based on TDOAs, the noise covariance matrix Σ that depends on the target location (x_T, y_T, z_T) is unavailable. As in the literature, we may set $\Sigma = I$ to compute an initial location solution $(\hat{x}_T^{(0)}, \hat{y}_T^{(0)}, \hat{z}_T^{(0)})$ via the constrained WLS procedure, which can then be substituted into Σ to compute the solution θ_{opt} to the corresponding constrained WLS. Although further iterations can be emplyed to obtain a more accurate solution, simulation results show that they are unnecessary. In fact, by Lemma 2, the component of FIM due to Σ, as in the Bang's formula, is insignificant compared to the first component, as in the Slepian formula, implying that the minimum achievable error variance by unbiased estimators is insensitive to the location parameter (x_T, y_T, z_T) embedded in Σ. Therefore, it is adequate to compute the solution to the constrained WLS twice.

5.3 Efficient Computation

An observation to the quasi-linear model (5.5) raises the question of model size reduction due to the $\mathbf{1}_L$ vector in the H matrix. Unfortunately,

$$\tilde{H} = \begin{bmatrix} \tilde{x}_{2,1} & \tilde{y}_{2,1} & \tilde{z}_{2,1} & \tilde{\Delta t}_2 \\ \vdots & \cdots & \cdots & \vdots \\ \tilde{x}_{n,1} & \tilde{y}_{n,1} & \tilde{z}_{n,1} & \tilde{\Delta t}_n \end{bmatrix}, \quad \tilde{a} = \begin{bmatrix} \tilde{a}_2 \\ \vdots \\ \tilde{a}_n \end{bmatrix}$$

does not exist, such that the constrained WLS in Theorem 1 with $\underline{a}, H, \Sigma$, and $\underline{\eta}$ in (5.5) is equivalent to the constrained minimization of

$$\tilde{J} = \frac{1}{2}(\tilde{a} - \tilde{H}\theta)'\tilde{\Sigma}^{-1}(\tilde{a} - \tilde{H}\theta).$$

However, memory complexity reduction can be achieved by computing and storing

$$H'\Sigma^{-1}H, \quad H'\Sigma^{-1}\underline{a}, \quad \underline{a}'\Sigma^{-1}\underline{a}, \tag{5.24}$$

which have much smaller dimensions than L, because the constrained WLS depends only on these three quantities. Indeed once the above three are available, the eigenvalue decomposition for $H'\Sigma^{-1}HQ^{-1}$, the polynomial in (5.20), the solution θ (dependent on Lagrange multiplies) in (5.16) , and the performance index in (5.15) can all be computed. So the judicious combination of the TDOA estimates in computing the near optimal localization estimate lies in these three quantities as well. Specifically, denote $W = \Sigma^{-1} = diag(w_2, \cdots, w_n)$, where

$$w_k = diag(w_{k;1}, \cdots, w_{k;L}), \quad \underline{w}_k = [\ w_{k;1} \quad \cdots \quad w_{k;L}\ ]'. \tag{5.25}$$

In light of the expression of Σ in (5.11), $w_{k;i}$ is approximately independent of i by (5.8), given

$$w_{k;i} = (2R_{k,T}c\sigma_k)^{-2} \ \ \forall \ \ i, \ \ 2 \le k \le n. \tag{5.26}$$

The expression in (5.26) is valuable. Introduce the inner products as

$$\begin{aligned}
(\mathbf{1}_L, \underline{w}_k) &= \sum_{i=1}^{L} w_{k;i} = \frac{L}{(2R_{k,T}c\sigma_k)^2}, \\
(c\Delta\underline{\hat{t}}_k, \underline{w}_k) &= \sum_{i=1}^{L} w_{k;i} c\Delta\hat{t}_{k;i} = \frac{L\overline{c\Delta\hat{t}_k}}{(2R_{k,T}c\sigma_k)^2}, \\
(w_k c\Delta\underline{\hat{t}}_k, c\Delta\underline{\hat{t}}_k) &= \sum_{i=1}^{L} w_{k;i}(c\Delta\hat{t}_{k;i})^2 = \frac{L\overline{(c\Delta\hat{t}_k)^2}}{(2R_{k,T}c\sigma_k)^2}, \\
(\underline{w}_k, \underline{a}_k) &= \sum_{i=1}^{L} w_{k;i} a_{k;i} = \frac{L\overline{a_k}}{(2R_{k,T}c\sigma_k)^2},
\end{aligned}$$

where $\overline{c\Delta\hat{t}_k}$ and $\overline{a_k}$ are simple averages of $\{c\Delta\hat{t}_{k;i}\}_{i=1}^{L}$ and $\{a_{k;i}\}_{i=1}^{L}$, respectively, and $\overline{(c\Delta\hat{t}_k)^2}$ is the squared average of the scaled TDOAs by c^2 given by

$$\overline{c\Delta\hat{t}_k} = \frac{1}{L}\sum_{i=1}^{L} c\Delta\hat{t}_{k;i}, \quad \overline{a_k} = \frac{1}{L}\sum_{i=1}^{L} a_{k;i}, \quad \overline{(c\Delta\hat{t}_k)^2} = \frac{1}{L}\sum_{i=1}^{L} (c\Delta\hat{t}_{k;i})^2, \tag{5.27}$$

respectively. Then it can be verified via a straightforward calculation

$$H'WH = \sum_{k=2}^{n} \begin{bmatrix} x_{k,1}^2(\mathbf{1}_L, \underline{w}_k) & x_{k,1}y_{k,1}(\mathbf{1}_L, \underline{w}_k) & x_{k,1}z_{k,1}(\mathbf{1}_L, \underline{w}_k) & x_{k,1}(c\Delta\underline{\hat{t}}_k, \underline{w}_k) \\ y_{k,1}x_{k,1}(\mathbf{1}_L, \underline{w}_k) & y_{k,1}^2(\mathbf{1}_L, \underline{w}_k) & y_{k,1}z_{k,1}(\mathbf{1}_L, \underline{w}_k) & y_{k,1}(c\Delta\underline{\hat{t}}_k, \underline{w}_k) \\ z_{k,1}x_{k,1}(\mathbf{1}_L, \underline{w}_k) & z_{k,1}y_{k,1}(\mathbf{1}_L, \underline{w}_k) & z_{k,1}^2(\mathbf{1}_L, \underline{w}_k) & z_{k,1}(c\Delta\underline{\hat{t}}_k, \underline{w}_k) \\ x_{k,1}(c\Delta\underline{\hat{t}}_k, \underline{w}_k) & y_{k,1}(c\Delta\underline{\hat{t}}_k, \underline{w}_k) & z_{k,1}(c\Delta\underline{\hat{t}}_k, \underline{w}_k) & (w_k c\Delta\underline{\hat{t}}_k, c\Delta\underline{\hat{t}}_k) \end{bmatrix},$$

$$= \sum_{k=2}^{n} \frac{L}{(2R_{k,T}c\sigma_k)^2} \begin{bmatrix} x_{k,1}^2 & x_{k,1}y_{k,1} & x_{k,1}z_{k,1} & x_{k,1}\overline{c\Delta\hat{t}_k} \\ y_{k,1}x_{k,1} & y_{k,1}^2 & y_{k,1}z_{k,1} & y_{k,1}\overline{c\Delta\hat{t}_k} \\ z_{k,1}x_{k,1} & z_{k,1}y_{k,1} & z_{k,1}^2 & z_{k,1}\overline{c\Delta\hat{t}_k} \\ x_{k,1}\overline{c\Delta\hat{t}_k} & y_{k,1}\overline{c\Delta\hat{t}_k} & z_{k,1}\overline{c\Delta\hat{t}_k} & \overline{(c\Delta\hat{t}_k)^2} \end{bmatrix},$$

$$H'W\underline{a} = \sum_{k=2}^{n} \begin{bmatrix} x_{k,1}(\underline{w}_k, \underline{a}_k) \\ y_{k,1}(\underline{w}_k, \underline{a}_k) \\ z_{k,1}(\underline{w}_k, \underline{a}_k) \\ (w_k c\Delta\underline{\hat{t}}_k, \underline{a}_k) \end{bmatrix} = \sum_{k=2}^{n} \frac{L}{(2R_{k,T}c\sigma_k)^2} \begin{bmatrix} x_{k,1}\overline{a}_k \\ y_{k,1}\overline{a}_k \\ z_{k,1}\overline{a}_k \\ \overline{a_k c\Delta\hat{t}_k} \end{bmatrix},$$

$$\underline{a}'W\underline{a} = \sum_{k=2}^{n}\sum_{i=1}^{L} a_{k;i}^2 w_{k;i} = \sum_{k=2}^{n} \frac{L\overline{a_k^2}}{(2R_{k,T}c\sigma_k)^2},$$

where $\overline{a_k^2} = \frac{1}{L}\sum_{i=1}^{L} a_{k;i}^2$ and $\overline{a_k c\Delta\hat{t}_k} = \frac{1}{L}\sum_{i=1}^{L} a_{k;i}^2 c\Delta\hat{t}_{k;i}$.

Remark 2. The efficient computation of the target location is hinged on the computation of the five averages $\{\overline{c\Delta\hat{t}_k}, \overline{(c\Delta\hat{t}_k)^2}, \overline{a_k}, \overline{a_k^2}, \overline{a_k c\Delta\hat{t}_k}\}$. Once these five averages are available, $H'WH, H'W\underline{a}$, and $\underline{a}'W\underline{a}$ are also available, as long as the sensor locations are known. Note that TDOAs and $\{\sigma_k\}$ are always scaled by the speed of light c to avoid a numerical problem in the case of finite digits because TDOAs and $\{\sigma_k\}$ are very small while c is very large. Hence, efficient computation and reduction of storage complexity can both be achieved. Since $R_{k,T}$ is unknown, the weighting matrix W can be set to I in the first use of the localization algorithm. After an initial estimate of the target location is available, approximate $R_{k,T}$ for $2 \leq k \leq n$ can be computed and used for the weighting W. Our algorithm requires at least twice the use of the same localization algorithm.

It is noted that the constrained WLS solution is an approximate MLE solution to the source localization problem based on TDOAs by treating measured TDOAs $\{\Delta\hat{t}_{k;i}\}$ as deterministic quantities. That is, it is an approximate MLE solution conditioned on the measured TDOAs. However it is also important to observe that even if we treat $\Delta\hat{t}_{k;i}$ as random, the constrained WLS solution is still an approximate MLE solution, due to the fact that the constrained WLS solution is optimal for all TDOA estimates under the Gauss assumption.

5.4 Simulation Studies

Example 1 Consider the indoor localization inside a building. The seven different WiFi receivers available acted like sensors in the locations specified by their Cartesian coordinates tabulated as seen in Table 5.1.

Table 5.1 The location coordinates of the WiFi receivers

Coordinates	$k=1$	$k=2$	$k=3$	$k=4$	$k=5$	$k=6$	$k=7$
x	100	125	87.5	112.5	137.5	100	125
y	50	50	37.5	37.5	37.5	25	25
z	2	10	18	10	2	2	18

It is noted that the x-coordinates range from 100 to 137.5 meters, the y-coordinates range from 25 to 50 meters, and the z-coordinates range from 2 to 18 meters. The target is assumed to have the location coordinates $(x_T, y_T, z_T) = (110, 45, 1)$. The TDOA estimates are given as

$$c\widehat{\Delta t}_{k,1} = R_{k,T} - R_T + c\eta_k, \qquad 1 < k \leq n = 7,$$

with c the speed of light, $R_{k,T}$ being the distance from the kth sensor to the target, $R_T = R_{1,T}$, and η_k as the estimation error. In this simulation study, we assume that η_k is Gauss distributed with

$$\mathrm{E}\{c\eta_k\} = 0, \qquad \mathrm{E}\{c\eta_k^2\} = c^2\sigma_k^2,$$

and $c\sigma_k$ is proportional to the product of the distances $R_{k,T}$ and R_T because the TDOA estimates are obtained from correlation, involving product of the two received signals. The following is the product of $R_{k,T}$ and R_T for $2 \leq k \leq n = 7$:

$$204.2205, \quad 327.5500, \quad 134.4656, \quad 320.1578, \quad 251.2489, \quad 339.3582.$$

So, we set $c\sigma_k = \mu R_{k,T} R_T$, where $0.1 \leq \mu \leq 1$ with unit meter. Since 10 nano-seconds correspond to approximately 3 meters, the standard deviations for $0.1 \leq \mu \leq 1$ represent close to $0.1 \sim 1$ microsecond estimation errors for TDOA. Considering that the channel bandwith for WiFi 802.11 is 20 MHz, the standard deviation of $0.1 \sim 1$ microsecond as the TDOA estimation error is reasonable. We generated $N = 1000$ ensembles of the TDOA estimation errors in Gauss distribution in each trial with $\mu \in [0.1, \ 1]$ fixed. The root-mean squared error (RMSE) of the localization errors is plotted in Figure 5.1 for $0.1 \leq \mu \leq 1$.

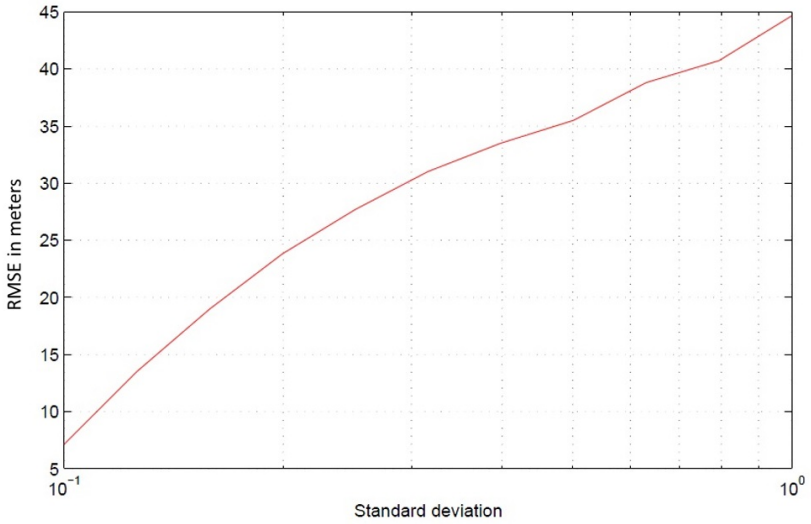

Figure 5.1 RMSE of the target location error versus μ using all TDOA estimates

The RMSE of the location error is computed according to

$$\text{RMSE} = \sqrt{\frac{1}{N}\sum_{i=1}^{N}[(\hat{x}_{T_i} - x_T)^2 + (\hat{y}_{T_i} - y_T)^2 + (\hat{z}_{T_i} - t_T)^2]}$$

with $(\hat{x}_{T_i}, \hat{y}_{T_i}, \hat{z}_{T_i})$ as the ith estimate for the target location. It is noted that we assume 100 different TDOA estimates, $\widehat{\Delta t}_{k,1}$, are available at each of the $(n-1)$ sensor locations. So, in effect, we have 600 TDOA estimates for target localization. The reason for using 100 TDOA estimates lies in the time-division and frequency division approach. With 10 different non-overlapping time subintervals and 10 different frequency subbands (each having a bandwidth of 2 MHz), we have 100 TDOA estimates at each of the $(n-1)$ sensor locations.

We also tested the localization error using the mean of the TDOAs at each of the $(n-1)$ sensors and then use the localization algorithm to find the target location. Surprisingly, this simple method gives us much better performance for the location error as shown in the next figure, even though this simple method is not close to optimal.

The location performance is often measured by the outage curve [2]. So, we examined the case when $\mu = 0.3$, at which the location errors in Figure 5.1 and Figure 5.2 are very close to each other. The outage curve is shown in Figure 5.3.

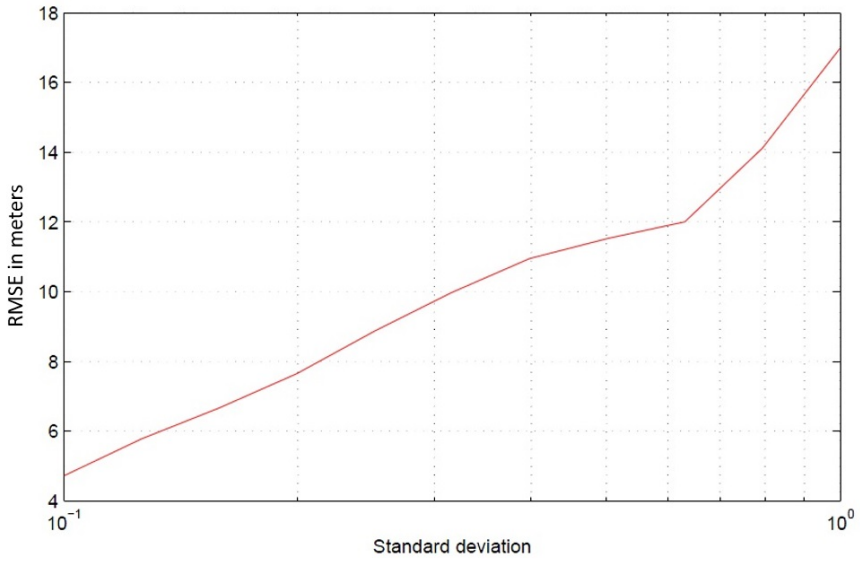

Figure 5.2 RMSE of the target location error versus μ with simple average for TDOA

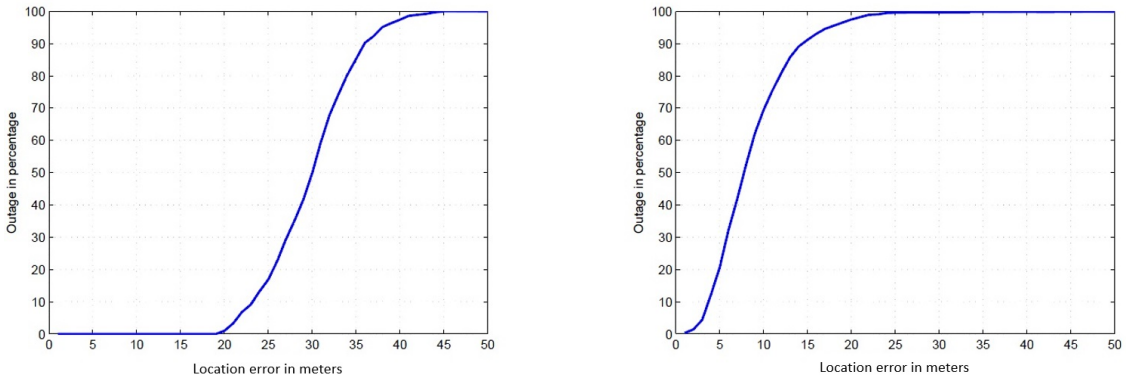

Figure 5.3 Outage curve with near optimal algorithm (left) and with simple average (right)

The outage curves show again that the algorithm based on a simple average of TDOA estimates prior to applying the near optimal location algorithm performs better. For instance, 90% of the target estimates are within 15 meter location errors for the figure on the right but are within 35 meter location errors for the figure on the left.

Example 2 The second example considers the outdoor localization, assuming the RF sensor locations given in Table 5.2:

Table 5.2 The location coordinates of the RF receivers

Coordinates	$k=1$	$k=2$	$k=3$	$k=4$	$k=5$	$k=6$	$k=7$
x	0	1750	1750	-1750	-1750	0	0
y	0	1000	-1000	1000	-1000	2000	-2000
z	28	54	12	32	14	8	10

The target is assumed at $(x_T, y_T, z_T) = (537, -785, 1.7)$. The standard deviation for $c\widehat{\Delta}t_{k,1}$ is computed in the same way as earlier, assumed to be proportional to the product of the two distances. We scale these values to some appropriate values shown below:

$$41.0801,\ \ 23.4431,\ \ 55.2096,\ \ 43.7125,\ \ 53.9729,\ \ 25.2786. \tag{5.28}$$

The above values are smaller than the previous indoor example because the multipath is much less severe for the outdoors. We again use $\mu \in [0.1,\ 1]$ to scale the above standard

deviations and assume 100 TDOA estimates are each of the $(n-1)$ sensors. Figure 5.4 shows the localization error in the RMSE value for the near optimal algorithm with a blue dot-dashed line and for the algorithm based on simple average a solid red line.

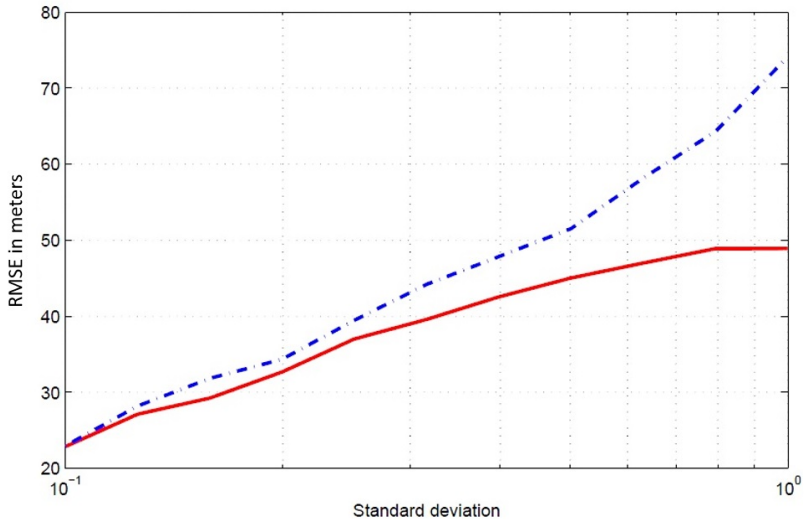

Figure 5.4 RMSE of the location error versus μ for outdoor target

Again the localization algorithm based on the simple average of the TDOAs performs better than the more complicated near optimal algorithm in terms of the average localization error although they differ little from each other at low noise intensity.

Similar to the previous example, we also examine the outage performance for outdoor localization using half of the same standard deviation as in the results in (5.28). The results are summarized in Figure 5.5. The outage curves again show that the algorithm based on the simple average of the TDOA estimates performs better than the near optimal algorithm.

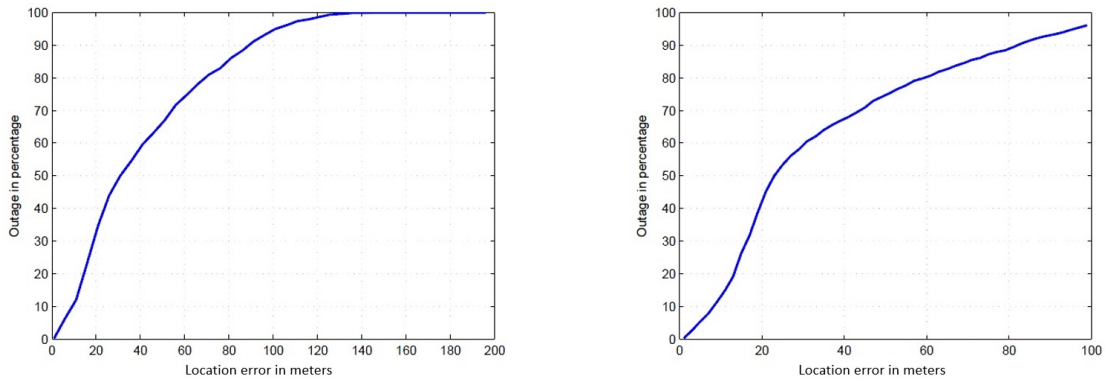

Figure 5.5 Outage curve with near optimal algorithm (left) and with simple average (right)

5.5 Application of Estimated TDOA

This section summarizes the localization simulation using the estimated TDOAs as studied in Chapter 4. In the previous section, we used randomly generated TDOA estimation values for our simulation study.

We use the same location for the target and sensors as in Example 1 in Chapter 5.4, considering indoor localization (inside a building). Figure 5.6 shows the simulation results. The figure on the left is the simple average algorithm in the previous section where L=100 and 200 ensembles. The figure on the right is the averaged estimated TDOA of 8 sub-bands at each sensor pairs as shown in Table 4.1 with 200 ensembles.

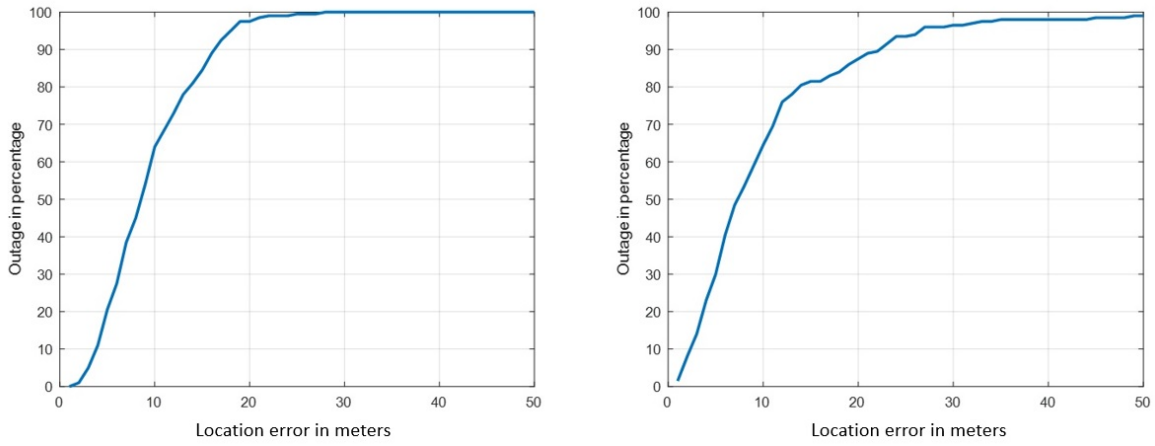

Figure 5.6 Outage curve with randomly generated TDOAs (left) and with estimated TDOAs (right)

The performance is very similar when error is smaller than 10 meters but becomes worse when the error increases. The possibility of the difference between them is that the left one has much more TDOA estimates at each pair of sensors. In addition, the randomly generated TDOAs are Gauss distributed, but the estimated TDOAs based on WiFi signals may not have so nice a distribution as Gauss.

Figure 5.7 shows the outage curve simulation results with estimated TDOAs from Table 4.2. The estimated TDOAs in SNR 50 dB are very close to the true TDOAs and have a ve-

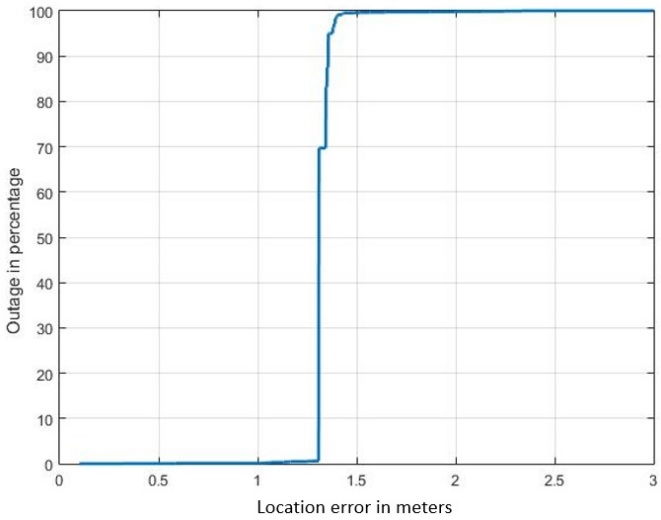

Figure 5.7 Outage curve with estimated TDOAs

ry small detection error and standard deviation. So, almost 100% of the target estimates are within the 1.5 meter location errors.

CHAPTER 6
CONCLUSION

In this thesis, we presented our work on wireless localization in the absence of GPS. This research has been focused on localization using the WiFi signal because it has been widely used inside buildings in which the GPS signal is not available or too weak to obtain an accurate location.

According to the IEEE 802.11 technology, OFDM is a digital multicarrier modulation method used in WiFi. We use OFDM symbols as an opportunistic RF signal for wireless localization. Both WiFi and OFDM are introduced in Chapter 2. Our preliminary study for the use of the WiFi signal to localize mobile targets is carried out in Chapter 3, focusing on symbol detection and channel estimation. The simulation results show that the symbol detection error and channel estimate error are functions of the SNR. As the SNR increases, both errors decrease, which is well-known. Kalman filtering is also employed for channel estimation by assuming the AR WSSUS channel model, and it achieves better performance especially in the case of a low SNR.

A first step for localization based on transmitted WiFi signals from the target is to estimate the TDOA from at least four receivers. WiFi signals are wide-band in nature and induce multipath phenomena that hinder the TDOA estimation. Hence, in Chapter 4, a subband division method is proposed to divide the WiFi signal into multiple non-overlapping subband signals for which the multipath effect is greatly reduced. In addition, a time division method is proposed to divide the WiFi signals into multiple non-overlapping sub-signals in the time domain to mitigate the clock drift. The simulation results show that the frequency and time division methods provide quite accurate TDOA estimation results.

Wireless localization based on TDOA estimates at $n \geq 4$ sensors was investigated in Chapter 5. This is a nonlinear estimation problem. It is shown in this thesis that the nonlinear term treated as a constraint is thus converted into a quasi-linear form that is in fact a quadratic constraint. A numerical procedure based on simultaneous diagonalization is

developed to compute the WLS solution under the quadratic constraint. This new procedure is shown to be an approximate MLE solution under the hypothesis (5.9), which holds true approximately in practice. We also studied how to combine the multiple TDOA estimates at each pair of the n sensors judiciously in computing the optimal target location estimate. As concluding remarks, we comment that the assumption on uncorrelated TDOA measurement noises can be removed. Such an assumption is in fact not used in deriving the constrained WLS solution. That is, the solution procedure summarized in Theorem 1 is applicable to the case when it is an arbitrary symmetric positive definite matrix. See also the results in [4] for the derivation of the various covariance matrices when the TDOA measurement noises are correlated. We also comment that the moving source localization studied in [11] involves two quadratic constraints to which a similar constrained WLS solution can be derived. However, it involves roots computation for two 2-variate polynomials, which have a high complexity, and is susceptible to noise corruption. The efficient computation is also investigated in Section 5.3. Our simulation results show that the use of the averaged TDOA estimates has better performance for both indoor and outdoor localization. Possible reasons may lie in the numerical issue and the non-Gauss distributed errors in the pseudo-linear model.

While this thesis work summarizes our work on wireless localization, further research is needed in order for our proposed algorithms to work well in practice. We list two important future research problems below:

1. The performance limitation: The fundamental limit for localization based on TDOA estimates remains unknown. Even though Cramér-Rao lower bounds can be derived and analyzed, they are based on Gauss assumption that do not hold in practice.

2. The computation complexity: While numerical efficient algorithms are studies in this thesis, wireless localization based on TDOAs is inherently complex. Indeed both TDOA estimates and location estimates are difficult to compute.

It is believed that both of the above problems are attributed to nonlinearities of the

TDOAs as functions of the location. How to combat the nonlinearities and improve the location performance belongs to the category of nonlinear estimation that is extremely difficult to tackle. We hope that this thesis sheds some light on this difficult problem.

REFERENCES

[1] J.S. Abel and J.O. Smith. Source range and depth estimation from multipath range difference measurements. *IEEE Trans.Acoust.Speech, Signal Processing*, 37(11):1157–1165, 1989.

[2] P. Bahl and V.N. Padmanabhan. RADAR: an in-building RF-based user location and tracking system. In *19th Annual Joint Conference of the IEEE Computer and Communications Societies (INFOCOM00)*, volume 2, page 775784, March 2000.

[3] G.C. Carter. Time delay estimation for passive sonar signal processing. *IEEE Trans. Acoust. Speech, Signal Processing*, 29:463–470, June 1981.

[4] E.C.L. Chan, G. Baciu, and S.C. Mak. Using Wi-Fi signal strength to localize in wireless sensor networks. In *Int. Conf. Commun. Mobile Comput.*, 2009.

[5] Y.T. Chan and K.C. Ho. A simple and efficient estimator for hyperbolic location. *IEEE Trans. Aerosp. Electron. Syst.*, 26:748–753, Sept. 1990.

[6] W.H. Foy. Position-location solutions by Taylor-series estimation. *IEEE Trans. Aerosp. Electron. Syst.*, 12:187–194, Jan. 1987.

[7] B. Friedlander. A passive localization algorithm and its accuracy analysis. *IEEE J. Ocean. Eng.*, 12:234–245, Jan. 1987.

[8] G. Gu. Advanced localization based on multiple TDOA estimates. Technical report, ECE, LSU, January 2015.

[9] W.R. Hahn and S.A. Tretter. Optimum processing for delay-vector estimation in passive signal arrays. *IEEE Trans. Inform. Theory*, 19:608–614, Sept. 1973.

[10] K.C. Ho and W. Xu. An accurate algebraic solution for moving source location using TDOA and FDOA measurements. *IEEE Trans. Signal Processing*, 52:2453–2463, Sept. 2004.

[11] R.A. Horn and C.R. Johnson. *Matrix Analysis*. Cambridge University Press, 1999.

[12] H.D. Kang and G. Gu. Simulation studies for localization based on TDOA estimates. Technical report, ECE, LSU, February 2015.

[13] H.D. Kang and G. Gu. Simulation studies for OFDM channel estimation and symbol detection. Technical report, ECE, LSU, April 2015.

[14] H. Rohling. *OFDM Concepts for Future Communication Systems*. Springer, 2011.

[15] A.H. Sayed, A. Tarighat, and N. Khajehnouri. Network-based wireless location. *IEEE Signal Processing Magazine*, 22:24–40, July 2005.

[16] H.C. Schau and A.Z. Robinson. Passive source localization employing intersecting spherical surfaces from time-of-arrival differences. *IEEE Trans. Acoust. Speech, Signal Processing*, 35:1223–1225, Aug. 1987.

[17] J.O. Smith and J.S. Abel. Closed-form least-squares source location estimation from range-difference measurements. *IEEE Trans. Acoust. Speech, Signal Processing*, 35:1661–1669, Dec. 1987.

[18] P. Stoica and R. Moses. *Introduction to Spectral Analysis*. Prentice-Hall, 1997.

[19] D.J. Torrieri. Statistical theory of passive location systems. *IEEE Trans. Aerosp. Elect. Syst.*, 20:183–198, Mar. 1984.

[20] Wikipedia. IEEE 802.11 - Wikipedia, the free encyclopedia, 2016. [Online; accessed 22-March-2016].

VITA

Hyundeok Kang was born in Seoul, South Korea. He completed his Bachelor's and Master's Degree in Electronic Engineering at Inha university, Incheon, South Korea in 2007 and 2010, respectively. In the fall of 2014, he joined the Department of Electrical and Computer Engineering at Louisiana State University, Baton Rouge, in pursuit of his graduate study, focusing on Systems Control. He anticipates to be awarded the Master's Degree of Science in Electrical Engineering in August 2016.